

1 **Second-order hydrodynamic effects on the response of** 2 **three semisubmersible floating offshore wind turbines**

3 Lixian Zhang ¹, Wei Shi ^{1,2,*}, Madjid Karimirad ³, Constantine Michailides ⁴ and Zhiyu Jiang ⁵

4 ¹DeepWater Engineering Research Centre, Dalian University of Technology, China;

5 ²State Key Laboratory of Hydraulic Engineering Simulation and Safety, Tianjin University, China;

6 ³Civil Engineering, School of Natural and Built Environment, Queen's University Belfast, UK;

7 ⁴ Civil Engineering and Geomatics, Cyprus University of Technology, Cyprus;

8 ⁵ Department of Engineering Sciences, University of Agder, Grimstad, Norway;

9 * Corresponding author: Dr. Wei Shi, Email: weishi@dlut.edu.cn

10 **Abstract:** Floating structures have become the most feasible solution for supporting wind
11 turbines when offshore wind project move to deeper water. In this paper, a hydrodynamic
12 analysis of three different semisubmersible floating offshore wind turbines is carried out
13 including second-order hydrodynamic effects. The three examined platforms are V-shaped
14 semisubmersible, Braceless semisubmersible and OC4-DeepCwind semisubmersible and
15 are used to support the NREL 5 MW reference wind turbine. The main objective of the
16 present study is to investigate and compare the hydrodynamic response of the three
17 different semisubmersible floaters in two water depths (100 m, and 200 m) under different
18 load conditions. The effects of second-order wave loads on the platform motions and
19 mooring tension are discussed and compared by using different methods including
20 Newman's approximation and the full QTF (Quadratic transfer function) method. The drag
21 effect on the structure motion response is also discussed in this paper. The comparison
22 presented is based on statistical values and response spectra of floating platform motions as
23 well as mooring tensions. The results show that the dynamic response of semisubmersible
24 FOWTs (floating offshore wind turbines) is overestimated when ignoring the Morison drag
25 effect on the columns of the semisubmersible FOWT. The second-order difference wave
26 loads can excite the resonance of motion especially for the platform-pitch motion, which
27 could cause structural failures. The full QTF method should be used to calculate the second-
28 order wave force to better simulate the realistic dynamic response of semisubmersible
29 FOWTs.

30 **Keywords:** Hydrodynamic loads; Second-order wave loads; Semisubmersible floating wind
31 turbines; Newman's approximation; Quadratic transfer function.

32 1. Introduction

33 Wind energy has experienced rapid development in recent years, moving from onshore to
34 offshore. At the end of 2018, 18,499 MW of installed wind turbine power capacity from a total
35 of 4,543 offshore wind turbines was installed (DeCastro *et al.*, 2019). Most offshore wind
36 turbines are installed in shallow water with bottom-fixed foundations (Shi *et al.*, 2015, 2016;
37 Mo *et al.*, 2017; Chian *et al.*, 2018). In many countries, including China, Norway and the USA,
38 the main portion of offshore wind resources is found in deep water, where the bottom-fixed
39 supporting structures are not economically feasible. Floating offshore wind turbines
40 (FOWTs) provide a promising solution in deep water areas. In China, the offshore resources
41 in shallow water are estimated to be 750 GW at 10 m height, while the offshore resources in
42 deep water are estimated to be 1740 GW (Hong and Möller, 2011). To explore the wind
43 energy in deep water sites, many concepts have been proposed for FOWTs, by utilizing
44 technology and experience from the offshore oil and gas industry. Based on the principles
45 adopted to achieve static stability, floating support platforms can be classified into three
46 primary concepts: semisubmersible, spar buoy and Tension Leg Platform (TLP). Some
47 designs are in the prototype stage including the full-scale projects Hywind demo (Driscoll *et*
48 *al.*, 2016) in Norway, WindFloat (Maciel, 2010) in Portugal, Fukushima phase II FOWT
49 (Boccard, 2014) in Japan and Hywind Scotland (Skaare, 2017) in the UK etc. Compared to
50 spar buoy and TLP, the semisubmersible platform is more feasible in various water depths
51 and has low installation costs of the mooring system. The semisubmersible platform has
52 better hydrodynamic behaviour due to the deep draft. Several concepts of semisubmersible
53 floating offshore wind turbines have been proposed including WindFloat (Roddier *et al.*,
54 2010), Dutch Tri-floater (Huijs *et al.*, 2014), Windsea (Lefranc *et al.*, 2011), Windflo (Le
55 Boulluec *et al.*, 2013), Braceless (Luan *et al.*, 2016), V-shaped (Karimirad and Michailides,
56 2015), OC4-DeepCwind (Robertson *et al.*, 2014) semisubmersible FOWTs.

57 Currently, several numerical simulations of FOWTs (Antonutti *et al.*, 2016; Jiang *et al.*, 2018;
58 Shi *et al.*, 2019; Zhao *et al.*, 2019) have been carried out to investigate the dynamic
59 performance of semisubmersible FOWTs using first-order radiation and diffraction. However,
60 the offshore oil and gas industry has demonstrated the importance of second-order
61 hydrodynamic load for certain floating platform. The second-order wave loads mainly include
62 mean drift force, sum- and difference-frequency wave loads. The sum-frequency and
63 difference-frequency loads can excite offshore structures' eigenfrequencies, and may result
64 in large oscillations that cause damage to the floating structures. Roald *et al.* (2013)
65 assessed the importance of second-order wave forces on OC3-Hywind spar and the UMaine

66 TLP. The results show that the second-order wave forces are very small for OC3-Hywind,
67 while those are quite high on UMaine TLP. Coulling et al.(2013) used Newman's
68 approximation method in FAST to consider the effect of second-order wave force on OC4-
69 DeepCwind semisubmersible FOWT. The results show that the second-order difference-
70 frequency wave-diffraction forcing played a significant role in the global response of the
71 DeepCwind semi-submersible FOWT. Li et al. (2017) proposed a new concept of FOWT and
72 investigated the hydrodynamic response of the floating platform with an emphasis on the
73 computation of second-order difference-frequency wave loads and their effects on the global
74 rigid-body motion response. Xu et al. (2018) assessed the importance of second-order
75 hydrodynamics on the Braceless semisubmersible floating offshore wind turbine concept
76 using Newman's approximation and the full QTF method. Gueydon et al. (2014) used
77 different codes including FAST and aNySIM to investigate the second-order effect on OC4-
78 DeepCwind semisubmersible FOWT. The results show that the second-order sum-frequency
79 loads appeared to have negligible effects on the motions while the effects of difference-
80 frequency load were larger. The loads and responses of the system caused by the second-
81 order hydrodynamics were analyzed and compared to the first-order hydrodynamic loads
82 and induced motions in the frequency domain by Bayati et al (2018).

83 In this paper, the main objective is to investigate hydrodynamic effects on the response of
84 three different semisubmersible floating offshore wind turbines, including the V-shaped
85 semisubmersible FOWT, the Braceless semisubmersible FOWT and the OC4-DeepCwind
86 semisubmersible FOWT, at different water depths addressing second-order hydrodynamic
87 loads. Hydrodynamic models are developed by using the ANSYS/AQWA tool with the panel
88 method (ANSYS Inc., 2017). Particular attention is given to second-order hydrodynamics
89 loadings using Newman's approximation and the full QTF method. **The second-order**
90 **hydrodynamic loads** and resulted responses are analyzed and compared with relevant
91 loads, responses and induced motions in the frequency-domain for different water depths.
92 The effect of the second-order hydrodynamic loads and water depth is examined for all three
93 semisubmersible platforms.

94 **In moderate water depths (40 m to 100 m), dynamic responses of semisubmersible FOWT**
95 **become larger than those in deep water. For the responses of the three semisubmersible**
96 **FOWTs at different water depth, the results show that the Braceless semisubmersible FOWT**
97 **is more sensitive in shallow water depth.** For the first-order solution, Morison drag term has a
98 significant impact on the platform motion showing that Morison drag term should also be
99 considered for better simulating the actual motion responses. **Furthermore, it is found that**

100 the heave natural frequency of OC4-DeepCwind semisubmersible FOWT is close to the
101 normal wave frequency range, which could cause large resonance and then cause the
102 failure of the structure. For second-order solution, motion responses can be excited when
103 considering second-order wave loads. The results show that the pitch motion can be greatly
104 excited when using the full QTF method. Compared to the pitch motion responses of three
105 semisubmersible FOWTs at different water depth, the contribution of second-order wave
106 loads to the pitch motion increasing when the water depth decreases. Therefore, the full
107 QTF method should be used in the numerical simulation of semisubmersible FOWTs to
108 better capture the effect of second-order wave loads. The results presented in this paper
109 may help resolve the fundamental design trade-offs between different FOWTs.

110 2. Theoretical background

111 It is important to design floating offshore wind turbines considering fluid-structure-interaction.
112 The force on the floating structures and motion of the platform caused by these interactions
113 is one of the main subjects of marine hydrodynamics. The hydrodynamics are mainly divided
114 into two parts: the influence of fluid motions on the structures (diffraction), and the influence
115 of moving structures that lead to the wave generation (radiation). Hydrostatics should also
116 be accounted for to consider the effects of buoyancy and hydrostatic restoring forces. The
117 hydrodynamic loads can be estimated by using the Morison equation, potential flow theory,
118 hybrid methods or higher fidelity numerical modelling techniques (e.g. computational fluid
119 dynamics (CFD)). The Morison Equation is mainly used to calculate the hydrodynamic loads
120 for slender structures with small diameters compared with the wavelength. For large-volume
121 structures, diffraction and radiation are relatively important and potential flow theory is used
122 to calculate the hydrodynamic loads acting on the platform.

123 2.1 Potential flow theory

124 The potential flow theory (Faltinsen, 1993; Teng, 2015) is used to calculate the
125 hydrodynamics when designing marine structures. Potential flow theory considers the flow
126 around a body to be incompressible, inviscid, and irrotational, with negligible surface-tension
127 effects. The hydrodynamic loads that usually affect the response of floating wind turbines
128 consist of two parts: first-order wave loads and second-order wave loads.

129 2.1.1 First-order wave loads

130 For the first-order wave calculations, the load on the structure and platform motion have zero
131 mean value and oscillate with the frequency of the incident wave (Faltinsen, 1993). First-

132 order hydrodynamic wave load including incident wave loads, diffraction wave loads and
 133 radiation wave loads can be described by:

$$134 \quad \vec{F} = \vec{F}_I + \vec{F}_D + \vec{F}_R \quad (1)$$

$$135 \quad \vec{F}_I + \vec{F}_D = -\int_s i\omega\rho_w\phi_i\vec{n}_j ds - \int_s i\omega\rho_w\phi_d\vec{n}_j ds \quad (2)$$

$$136 \quad \vec{F}_R = -\ddot{x}_k \frac{\rho_w}{\omega} \int_s \phi_{ik}^{Re} \vec{n}_j ds - \dot{x}_k \rho_w \int_s \phi_{ik}^{Im} \vec{n}_j ds = -A_{jk} \ddot{x}_k - B_{jk} \dot{x}_k \quad (3)$$

137 where \vec{F}_I is the incident wave load; \vec{F}_D is the diffraction wave load; \vec{F}_R is the radiation wave
 138 load; ω is the circular frequency of the wave; \vec{n} is the normal direction vector of the wet
 139 surface; s is the area of the wet surface immersed in water; ϕ_i is the incident potential of
 140 the wave without the perturbation of the body; ϕ_d is the diffraction potential of the wave
 141 when the waves pass through the body; ρ_w is the density of the water; \vec{n}_j is a direction
 142 vector; ϕ_{ik}^{Re} and ϕ_{ik}^{Im} are the real and imaginary parts of the incident potential of the wave
 143 without the perturbation of the body, respectively; A_{jk} and B_{jk} are the added mass and
 144 radiation damping coefficients. The indices k and j refer to the degrees of freedom (DOFs)
 145 of the platform.

146 2.1.2 Second-order wave loads

147 Second-order hydrodynamic loads are proportional to the square of the wave amplitude and
 148 have frequencies that are equal to both the sum and the difference of pairs of incident wave
 149 frequencies. This means that, although the natural frequencies of the structure are designed
 150 to be outside the first-order wave energy spectrum, the second-order loads may excite these
 151 frequencies. Therefore, despite the normally small second-order hydrodynamic loads, the
 152 resonant effect may be significant. Second-order wave exciting forces can be described in
 153 the frequency domain by decomposition into three terms (Newman, 1967; Fonseca *et*
 154 *al.*,2008; Pessoa *et al.*, 2010):

155 (1) Mean drift force \bar{F}_{mean}^2 , which is a frequency-dependent mean value;

156 (2) Difference-frequency wave drift force \bar{F}_{diff}^2 , which oscillates at difference-wave
 157 frequencies;

158 (3) Sum-frequency wave force \bar{F}_{sum}^2 , which oscillates at sum-wave frequencies.

159 According to Pinkster (Pinkster, 1975), the second-order wave forces can be written as the
 160 summation of five different components when they are determined by direct pressure
 161 integration.

$$\begin{aligned}
 \bar{F}^2 = & -\oint_{WL} \frac{1}{2} \rho g \xi_r^{(1)} \cdot \xi_r^{(1)} \vec{n} dl & \text{I} \\
 & + \iint_{S_0} \frac{1}{2} \rho |\nabla \phi^{(1)}|^2 \vec{n} ds & \text{II} \\
 & + \iint_{S_0} \rho \left(X \cdot \nabla \frac{\partial \phi^{(1)}}{\partial t} \right) \vec{n} ds & \text{III} \\
 & + M_s R \cdot \ddot{X}_g & \text{IV} \\
 & + \iint_{S_0} \rho \frac{\partial \phi^{(2)}}{\partial t} \vec{n} ds & \text{V}
 \end{aligned} \tag{4}$$

163 where ρ is the density of the water; g is the gravitational acceleration; \vec{n} is The direction of
 164 the normal; $\phi^{(1)}$ is the first-order velocity potential; *WL is the waterline; $\xi_r^{(1)}$ is the relative*
 165 *wave elevation*; S_0 is the mean wetted surface of the floating body; X is the motion of the
 166 floating body; M_s is mass of the floating body; *M_s is the mass matrix of floating structure; R*
 167 *is the rotational transformation matrix of floating structure; \ddot{X}_g is the acceleration of the*
 168 *center of gravity; $\phi^{(2)}$ is the second-order velocity potential.*

169 Components I to IV represent the mean drift force which is determined from the first-order
 170 solution. The mean drift force can be calculated by using the far-field method or near-field
 171 method. The accuracy of the far-field method is higher than that of the near-field method, but
 172 it can calculate the force in only three DOFs. By contrast, near-field solution can be used to
 173 calculate second-order wave forces on a floating body in 6 DOFs. Therefore, the near-field
 174 method is employed in the present paper to calculate the mean drift force based on the
 175 mean wetted body surface integration approach.

176 **With** regards to the semisubmersible floating offshore platform, the slow drift wave force
 177 (term 5) including the difference-frequency force becomes more significant. The difference-

178 frequency is close to the natural frequency of the semisubmersible platform which could
 179 cause the resonance of the floating system and could damage the structure. The fifth
 180 component of equation (4) involves the second-order velocity potential that can be
 181 calculated directly by using the near-field solution (the full QTF method). Compared to
 182 Newman's approximation method, the complete QTF matrix gives more accurate estimations
 183 of the low-frequency loads; However, it requires the solution to the second-order problem
 184 and the time series reconstruction is more time-demanding. Therefore, Newman's
 185 approximation method is proposed, mainly to avoid computing the second-order velocity
 186 potential $\phi^{(2)}$ and to improve computational efficiency. For Newman's approximation, the
 187 drift force can be described by:

$$P_{ij}^- = 0.5a_i a_j \left(\frac{P_{ii}^-}{a_i^2} + \frac{P_{jj}^-}{a_j^2} \right) \quad (5)$$

$$Q_{ij}^- = 0 \quad (6)$$

where P_{ii}^- , P_{jj}^- , Q_{ii}^- and Q_{jj}^- are calculated from second-order mean drift force solution.

Therefore, quadratic transfer functions (QTF) including P_{ij}^- , Q_{ij}^- can be calculated.

For semisubmersible floating platforms, the most significant part of the dynamic response is at both the wave frequency and the structure natural frequency region. Therefore, only the mean drift force and slowly varying drift force will be discussed since the difference-frequency value is close to the natural frequency of the semisubmersible floating platform.

2.2 Viscous load

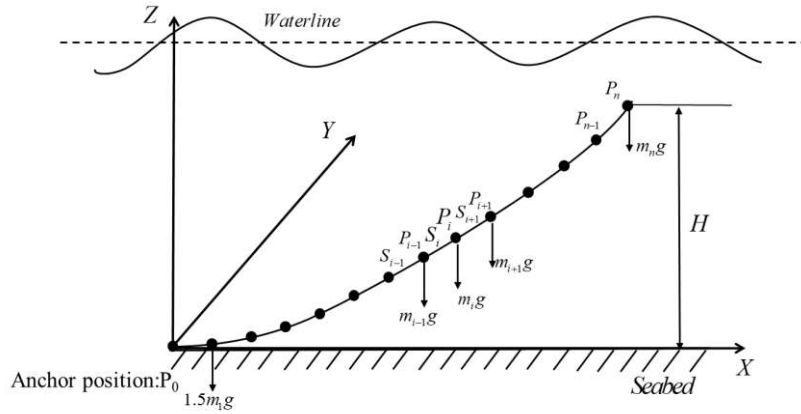
In the potential flow theory, the viscous effect from the flow is ignored. In order to take into account the viscous force, the drag term of the Morison equation is used. The viscous drag term of the Morison equation for the fluid force acting on the cross-section of a slender structural member is

$$dF_{viscous} = 0.5\rho C_d A |u_f - u_s| (u_f - u_s) dl \quad (7)$$

where C_d is the drag coefficient; A is the projected area of a unit length cylinder perpendicular to the flow direction; u_f is the fluid particle velocity; u_s is the structure's velocity.

205 2.3 Mooring system

206 In this paper, the lumped mass method (Hall and Goupee,2015) is adopted to discretize the
 207 cable dynamics over the length of the mooring line. In this approach, as seen in Figure 1, the
 208 mooring line is discretized into N evenly-sized line segments connecting N+1 node points.
 209 The right-handed inertial reference frame is defined with the Z-axis being measured positive
 210 up from the water plane. The location of each node point P_i which
 211 contains the node position in x, y and z-direction. Each segment S_i of a cable element has
 212 identical properties of unstretched length l , diameter d , density ρ , Young's modulus E , and
 213 damping coefficient C_{int} . And the cable model combines internal axial stiffness and damping
 214 forces with weight and buoyancy forces, hydrodynamic forces from Morison equation, and
 215 forces from contact with the seabed.



216
217 **Figure 1. Mooring line discretization**

218 2.4 Equation of motion

219 The semisubmersible floating structure is represented by a six degree of freedom (6-DOF)
 220 rigid body. The load model for the body accounts for the wave loads; It is stated that in the
 221 present paper, the emphasis is on the study of the hydrodynamic loads. The equation of
 222 motion under wave loads in time domain is calculated in ANSYS/AQWA; for the rigid body
 223 motions, j , and it can be expressed as:

$$224 \sum_{i=1}^6 \left((M_{ij} + A_{ij}) \ddot{x}_j(t) + \int_{-\infty}^t \dot{x}_j(\tau) K_{ij}(t-\tau) d\tau + C_{ij} \dot{x}_j(t) \right) = F_{wave,j}(t) + F_{moor,j}(t) \quad (8)$$

225 where M_{ij} is the mass coefficient, A_{ij} is the added mass coefficient calculated by AWQA-
 226 LINE, $K_{ij}(t-\tau)$ is the retardation function which represents the fluid memory effect, C_{ij} is the
 227 restoring coefficient calculated by AWQA-LINE, \ddot{x} , \dot{x} and x are the acceleration, velocity,

228 and displacement of the platform, $F_{wave,j}(t)$ is the wave exciting force, $F_{moor,j}(t)$ is the
 229 restoring force that results from mooring lines, j is the DOF in surge, sway, heave, roll, pitch
 230 and yaw direction.

231 3. Numerical model of the semisubmersible FOWTs

232 3.1 Wind turbine model

233 Different from the traditional marine floating structures, the large height of the wind turbine
 234 could cause instability of the floater. Although the wind effect is not included in the present
 235 paper which means the wind turbine is in a parked condition, the weight of wind turbines
 236 components is considered during the simulation. The wind turbine used in this paper was
 237 developed by the National Renewable Energy Laboratory (NREL), USA. It is a conventional
 238 three-bladed, upwind, variable-speed, collective-pitch controlled horizontal axis wind turbine.
 239 The geometric properties of the wind turbine and tower are listed in Table 1 (Jonkman *et al.*,
 240 2009).

241 **Table 1.** Main properties of NREL-5 MW baseline wind turbine and tower (Jonkman
 242 *et al.*, 2009).

Parameter	Value
Rated power	5 MW
Nacelle mass kg	240,000
Rotor mass kg	110,000
Wind turbine (WT) Center of Gravity(CoG) m	(-0.2,0.0,70)
Total mass of WT kg	600,000
Total WT mass moment of inertia about X axis(Ixx) kg*m ²	3,770,000,000
Total WT mass moment of inertia about Y axis(Iyy) kg*m ²	3,660,000,000
Total WT mass moment of inertia about Z axis(Izz) kg*m ²	112,000,000
Elevation to tower base above MSL m	10
Center of Gravity(CoG) location of tower above MSL m	43.4
Overall tower mass kg	250.,000

244 3. 2 Semisubmersible floating platform model

245 Three different semisubmersible floating platforms, including (1) the V-shaped
 246 semisubmersible floating platform, (2) the Braceless semisubmersible floating platform and
 247 (3) the OC4-DeepCwind semisubmersible floating platform, were considered to support the
 248 NREL 5 MW wind turbine at two different water depths. The water depth is assumed to be

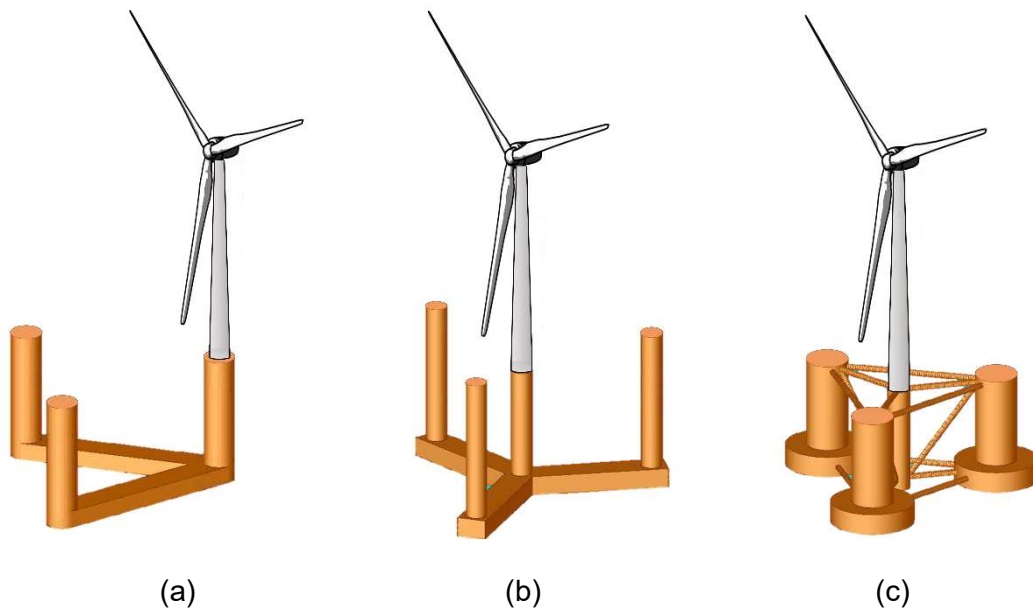
249 100 m and 200 m for each concept. The three floating structures are illustrated in Figure 2
 250 and their properties are summarized in Table 2.

251

252 Table 2. Properties for the three semisubmersible platforms.

Parameter	V-shaped Semi	Braceless Semi	OC4-DeepCWind Semi
Water depth m	200/100	200/100	200/100
Freeboard m	20	20	12
Draft m	28	30	20
Submerged volume m ³	10,013	10,517	13,917
Floater steel mass kg	1,630,000	1,686,000	3,852,000
Total mass (Including WT) kg	10,300,000	10,780,000	14,070,000
COG (x, y, z) m, m, m	(-30.6,0, -16)	(0,0, -18.9)	(0,0, -9.89)
I _{xx} w.r.t. COG kg*m ²	12,900,000,000	10,650,000,000	10,110,000,000
I _{yy} w.r.t. COG kg*m ²	21,800,000,000	10,650,000,000	10,110,000,000
I _{zz} w.r.t. COG kg*m ²	17,900,000,000	8,412,000,000	12,779,000,000

253



254

255

256

257 **Figure 2. Semisubmersible FOWT systems. (a) V-shaped Semi; (b) Braceless Semi; (c)**
 258 **OC4-DeepCwind Semi.**

259 The V-shaped semisubmersible FOWT is designed by Karimirad and Michailides (2015)
 260 according to the concept of semisubmersible FOWT in project Fukushima FORWARD
 261 (Forward, 2014). It consists of one main column and two side columns connected by two
 262 pontoons. Different from the other two semisubmersible platforms, V-shaped
 263 semisubmersible FOWT is not a symmetrical floating platform, which the NREL 5 MW wind
 264 turbine is at the top of the main column. It must be noted that V-shaped semi FOWT

265 maintains the balance by setting different ballast heights for each column. More detailed
266 properties of the V-shaped semisubmersible FOWT are summarized in (Karimirad and
267 Michailides, 2015; Karimirad and Michailides, 2016).

268 The Braceless semisubmersible FOWT is designed by Luan et al. (2016) in Norwegian
269 University of science and technology (NTNU) according to the concept of OO-Star
270 semisubmersible FOWT(Borisade, 2016). It is mainly composed of three side columns and
271 one central column. It is noted that the Braceless semisubmersible FOWT is symmetrical
272 with NREL 5 MW wind turbine on the centre column. Three pontoons are used to connect
273 central column and side columns. More detailed information of Braceless semisubmersible
274 FOWT can be found in (Luan, 2018).

275 The OC4-DeepCwind semisubmersible FOWT is designed by NREL. The OC4-DeepCwind
276 semisubmersible FOWT consists of one central column and three side columns. It has
277 heave plates at the bottom of the upper columns to reduce the heave motion of the floating
278 system. Several braces including horizontal and diagonal braces are used to connect the
279 columns. Detailed properties of the OC4-DeepCwind semisubmersible FOWT are available
280 in (Robertson et al., 2014).

281 The main reason we chose the aforementioned three semisubmersible FOWTs is that the
282 three semisubmersible FOWT represents different design ideas for semisubmersible FOWTs.
283 The V-shaped semisubmersible FOWT is an asymmetric structure without the bracings. And
284 both Braceless semisubmersible FOWT and OC4-DeepCwind semisubmersible FOWT is
285 symmetric structures with center column supporting the wind turbine systems. Different from
286 OC4-DeepCwind semisubmersible FOWT, Barceless semisubmersible FOWT has no
287 bracings to connect the center column and side columns. Those three semisubmersible
288 FOWTs are different in preliminary design.

289 3.3 Mooring systems designs for 200 m and 100 m

290 For the V-shaped semisubmersible FOWT, the mooring system consists of three catenary
291 mooring lines that are made of wire rope. The mooring line is positioned with 150 degrees
292 between the main mooring line (ML 1) and the side mooring lines (ML 2, ML 3), while the
293 angle between ML 2 and ML 3 is 60 degrees. The clump mass of the V-shaped
294 semisubmersible FOWT is positioned at 82 m far from the fairlead of each mooring line for
295 both 100 m and 200 m. The relevant characteristics of the mooring line are shown in Table 3
296 and 4.

297 The mooring system of Braceless semisubmersible FOWT consists of three catenary
298 mooring lines that are positioned with 120 degrees between the mooring lines. Each mooring
299 line is attached at the outer columns of the semisubmersible FOWT at a water depth of 18 m.
300 The clump masses of the Braceless semisubmersible for 100-m water depth are heavier
301 than those for 200-m water depth, which is designed to maintain the similar pretension and
302 stiffness in different water depths.

303 The initial OC4-DeepCwind semisubmersible FOWT is designed for 200-m water depth,
304 which has been utilized as a reference model for the mooring system design of 100-m water
305 depth. Based on the original 200-m water depth design, a 100-m water depth mooring line is
306 designed to achieve the similar stiffness (Jeon, *et al*, 2013), pretension and natural
307 frequency of the floating system in surge motion. The properties of the 100-m depth mooring
308 line are kept the same as those of the 200-m water depth mooring lines. A clump mass is
309 also added at each line to achieve similar pretension and stiffness. Detailed mooring line
310 properties and other characteristics of the mooring system are shown in Table 3 and 4.

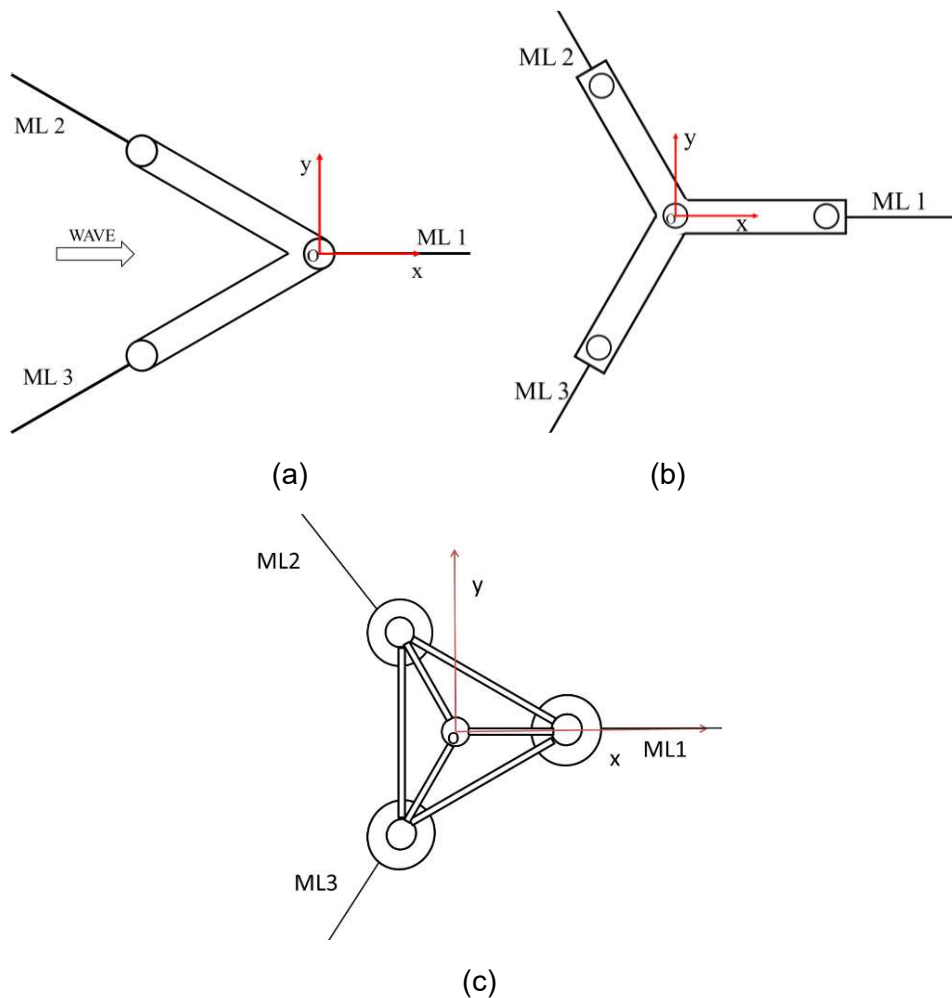


Figure 3. Mooring system configuration of the three platforms. (a) V-shaped Semi; (b) Braceless Semi; (c) OC4-DeepCwind Semi.

Table 3. Properties of the mooring line system at 200-m water depth.

Parameter	V-shaped Semi	Braceless Semi	OC4-DeepCWind Semi
Mooring line length m	700.0	1084.5	835.5
Mooring line type	Spiral rope	Spiral rope	Spiral rope
Number of mooring lines	3	3	3
Equivalent Axial stiffness N	3E9	3.08E9	7.536E8
Mass per unit length kg/m	117	115	108.63
Pretension kN	1680.0	1300.0	1040.0
Diameter of mooring line m	0.138	0.1365	0.0766
Fairlead for ML1 (x, y, z) m	(4.5, 0, -18)	(43, 0, -18)	(40.9,0, -14)
Fairlead for ML2 (x, y, z) m	(-55.8, -32.3, -18)	(-22.1, 38.3, -18)	(-20.4, -35.4, -14)
Fairlead for ML3 (x, y, z) m	(-55.8, 32.3, -18)	(-22.1, -38.3, -18)	(-20.4, 35.4, -14)
Anchor point of ML1 (x, y, z) m	(650, 0, -200)	(1084.4, 0, -200)	(-837.6, 0, -200)
Anchor point of ML2 (x, y, z) m	(-618.7, 357, -200)	(-542.2, 939.1, -200)	(-418.8, 725.4, -200)
Anchor point of ML3 (x, y, z) m	(-618.7,-357, -200)	(-542.2, -939.1, -200)	(-418.8, -725.4, -200)
Clump mass volume m ³	4.4	-	-
Clump mass weight kg	37,000	15,000	-

Table 4. Properties of the mooring line system at 100-m water depth.

Parameter	V-shaped Semi	Braceless Semi	OC4-DeepCwind Semi
Mooring line length m	453.0	891.6	514.0
Mooring line type	Spiral rope	Spiral rope	Spiral rope
Number of mooring lines	3	3	3
Equivalent Axial stiffness N	3E9	3.08E9	7.536E8
Number of mooring lines	3	3	3
Mass per unit length kg/m	117.00	115.00	108.63
Pretension kN	1500.0	1190.0	952.0
Diameter of mooring line m	0.138	0.1365	0.0766
Fairlead for ML1 (x, y, z) m	(4.5, 0, -18)	(43, 0, -18)	(40.9,0, -14)
Fairlead for ML2 (x, y, z) m	(-55.8, -32.3, -18)	(-22.1, 38.3, -18)	(-20.4, -35.4, -14)
Fairlead for ML3 (x, y, z) m	(-55.8, 32.3, -18)	(-22.1, -38.3, -18)	(-20.4, 35.4, -14)
Anchor point of ML1 (x, y, z) m	(434, 0, -100)	(917.0, 0, -100)	(535.0, 0, -100)
Anchor point of ML2 (x, y, z) m	(-433.7, 247, -100)	(-458.5, 794.1, -100)	(-267.5, 463.3, -100)
Anchor point of ML3 (x, y, z) m	(-433.7,-247, -100)	(-458.5, -794.1, -100)	(-267.5, -463.3, -100)
Clump mass volume/m ³	4.4	-	-
Clump mass weight/kg	37,000	15,000	45,000

3.4 Design load cases

Based on the data (Li., *et al*, 2015), Norway site 5 (Figure 4) was selected as a representative site for the simulation. It should be noted that wind loads are not considered in the present paper. The main objective of this paper is to investigate the hydrodynamic characteristics of different semisubmersible FOWT at different water depths with emphasis on the second-order wave loads. Therefore, only wave conditions are considered in the present paper. Three different wave conditions including moderate and extreme conditions are listed in Table 5.



Figure 4. Location of Norway site 5.

Table 5. Load cases for Norway site 5 (Li., *et al*, 2015).

Load case	Hs (m)	Tp (s)
LC 1	3.0	10.0
LC 2	5.0	12.0
LC 3	14.1	13.3

3.5 Numerical setting in the simulation

The hydrodynamic loads are calculated using the boundary element method (BEM) based on potential flow theory and the Morison equation. Potential flow theory is applied on both the columns and pontoons; and, the drag term of the Morison equation is applied to the columns. For the OC4-DeepCwind semisubmersible FOWT, the bracings are modelled using the Morison equation.

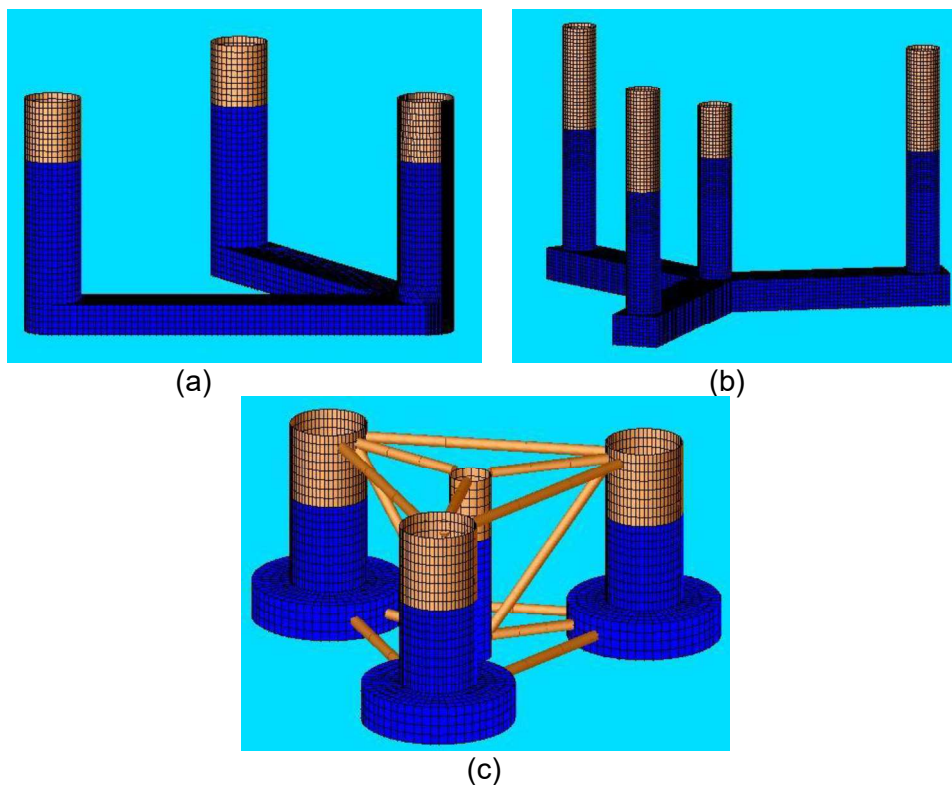
In this paper, first-order wave load analysis of the motion in sea states is performed with AQWA-NAUT (ANSYS Inc., 2017), which involves meshing the total wet surface of a structure to create a hydrodynamic and hydrostatic model. The nonlinear Froude-Krylov and hydrostatic wave forces on the instantaneous wetted surface (i.e., beneath the incident wave surface) can be calculated in NAUT. This calculation is performed at each time step, along

345 with the instantaneous values of all other forces. Accurate dynamic or kinematic properties
346 of fluid particles beneath the wave surface are thus required for this purpose. These forces
347 are then applied, via a mathematical model, see Equation (10). The position and velocity at
348 the subsequent time step are found by integrating these accelerations in the time-domain,
349 using a two-stage predictor-corrector numerical integration scheme.

350 For the second-order hydrodynamic model, the mean drift force can be calculated by using
351 the far-field method or near-field method in the AQWA-DRIF module (ANSYS Inc, 2017). In
352 AQWA-DRIF module, the QTF can be calculated by using the direct-pressure integration
353 method (Pinkster, 1975). Newman's approximation is also used to calculate the second-
354 order wave force.

355 3.5.1 Panel model

356 The panel model was developed in ANSYS software and the mapped mesh method is
357 employed to obtain a finer frequency domain simulation result for the semisubmersible
358 FOWTs in the AQWA-LINE module. The number of meshes used for the V-shaped
359 semisubmersible, the Braceless semisubmersible and OC4-DeepCwind semisubmersible
360 models are 11691, 23562 and 14735, respectively. The panel model of the three
361 semisubmersible numerical models is shown in Figure 5.



366 **Figure 5.** Panel model of the three platforms. (a) V-shaped Semi; (b) Braceless Semi model;
 367 (c) OC4-DeepCwind Semi.

368 3.5.2 Viscous drag model

369 To calculate the viscous drag of each column and pontoon on the semisubmersible FOWT
 370 by the Morison equation, a beam model was used in ANSYS software. Cd depends upon the
 371 Reynolds number, KC number, surface roughness and so on. According to Germanischer
 372 Lloyd standard (Wind, 2005), the Cd can be set to 0.70 when the Reynolds number is
 373 beyond 2.50E5. In the present simulation, the drag coefficient is set to 0.68 to simulate the
 374 viscous drag term on the columns and pontoons. It should be noted that the viscous force on
 375 the columns is applied along the transverse direction. Also, the axial viscous drag force is
 376 not considered in the present paper. The diameter of columns for the V-shaped
 377 semisubmersible (Figure 4(a)) and the Braceless semisubmersible (Figure 4(b)) FOWTs are
 378 9.0 m and 6.5 m respectively. For the OC4-DeepCwind semisubmersible FOWT (Figure
 379 4(c)), the diameters of the bracings, central column, upper column and base column is 1.6 m,
 380 6.5 m, 12.0 m and 24.0 m respectively. For the V-shaped semisubmersible FOWT and
 381 Braceless semisubmersible FOWT, the equivalent diameter of pontoons is 7.6 m and 8.3 m,
 382 respectively. The diameter of the columns and pontoons was set to 0.01 m to ignore the
 383 inertia force from the Morison equation. Furthermore, the drag coefficient is scaled to take
 384 into account the modified geometry of the beam model and maintain the same viscous effect
 385 contribution as in the real physical model. This is achieved by satisfying the following relation:

$$386 \quad C_d D = C'_d D' \quad (11)$$

387 where C'_d and D' are the equivalent drag coefficient and the diameter of the column in the
 388 beam model, respectively. The values used in the computation are shown in Table 6.

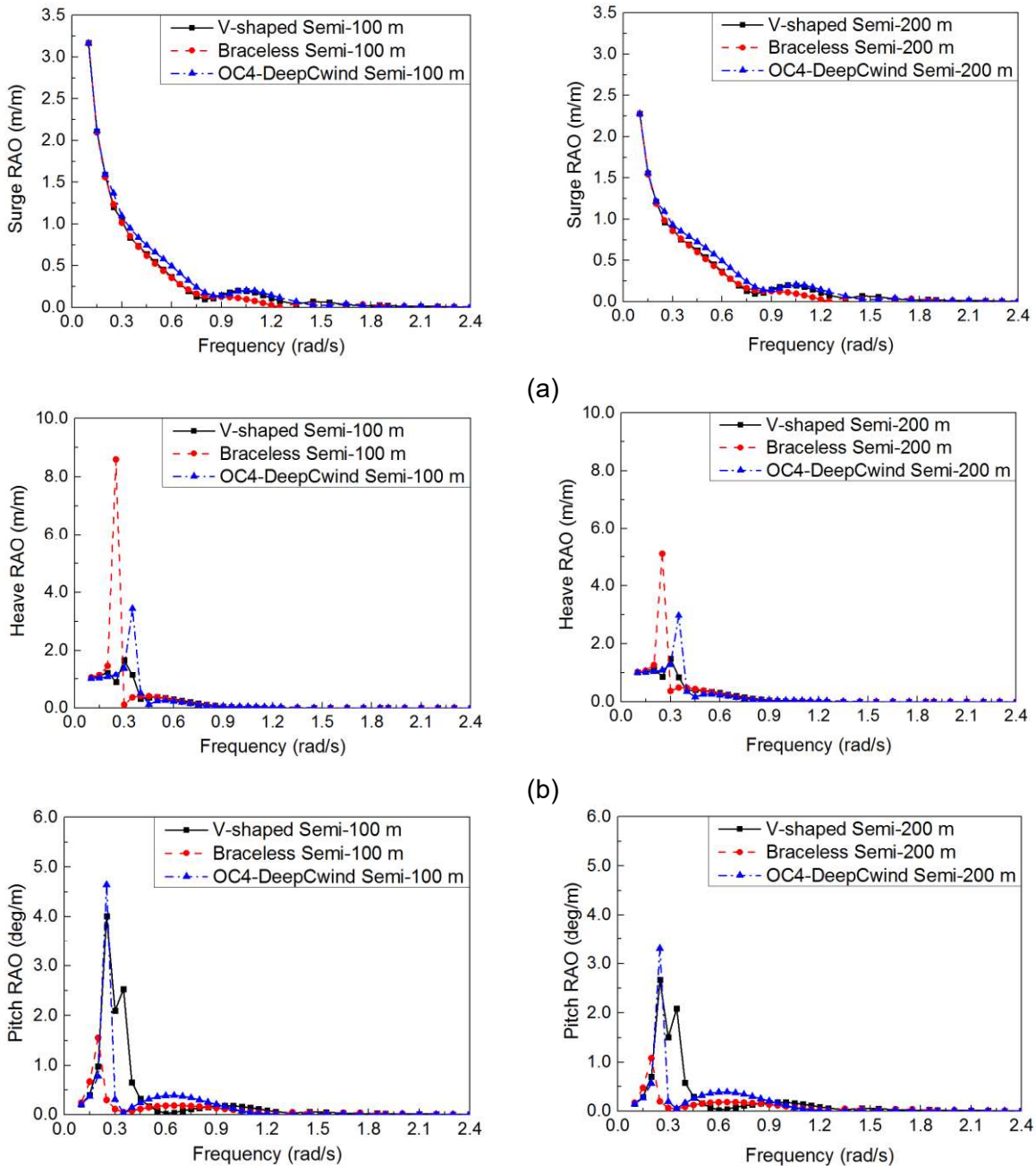
389 **Table 6.** Equivalent drag coefficients and diameters for the Morison model.

Parameters	V-shaped Semi		Braceless Semi		OC4-DeepCwind Semi			
	Column	Pontoon	Column	Pontoon	Braces	Center column	Upper column	Base column
C_a	-	-	-	-	1.0	-	-	-
C_d	0.68	0.68	0.68	0.68	0.68	0.68	0.68	0.68
C'_d	612.0	514.7	442.0	563.7	0.68	442.0	816.0	1632.0
D	9.0	7.6	6.5	8.3	1.6	6.5	12.0	24.0
D'	0.01	0.01	0.01	0.02	1.6	0.01	0.01	0.01

390 4. Result and discussion

391 **4.1 Response amplitude operator (RAO)**

392 Response amplitude operators (RAOs) can be computed based on the linear wave theory in
 393 AQWA. The RAOs show considerable excitation only in the surge, heave, and pitch modes,
 394 therefore only these RAOs are presented in Figure 6. The excitation at the other natural
 395 frequencies (sway, roll, and yaw) is considerably less because of the zero-degree wave
 396 heading.



401
 402
 403 Figure 6. RAOs of three semisubmersible FOWTs. (a) Surge; (b) Heave; (c) Pitch.

404 For the surge motion (Figure 6(a)), the results show that the RAOs are similar for the three
 405 semisubmersible FOWTs; however, the RAOs are larger at a water depth of 100 m than at a
 406 water depth of 200 m. For the heave motion (Figure 6(b)), two peaks are observed for the V-
 407 shaped semisubmersible FOWT showing the coupling effect between the heave and pitch
 408 motions. A large peak is presented for the heave response at the heave natural frequency of
 409 the Braceless semisubmersible FOWT, which is away from the incident wave frequency
 410 region (0.3 rad/s to 0.8 rad/s). One peak is also found at the heave natural frequency of the
 411 OC4-DeepCwind semisubmersible FOWT, which is close to the wave frequency region. This
 412 could cause a large heave motion response when the wave frequency is near the heave
 413 natural frequency of the OC4-DeepCwind semisubmersible FOWT. For the pitch motion
 414 (Figure 6(c)), there are two peaks observed in the low-frequency region which are in the
 415 heave and pitch natural frequency region, for the V-shaped semisubmersible FOWT, and
 416 one peak is found at the pitch natural frequency for both the Braceless and OC4-DeepCwind
 417 semisubmersible FOWTs. Notably, the pitch motion response in the wave frequency region
 418 of the OC4-DeepCwind semisubmersible FOWT is larger than that of the other two platforms.
 419 And it can also be observed that the heave and pitch motion responses for the three
 420 semisubmersible FOWTs are higher at moderate water depth.

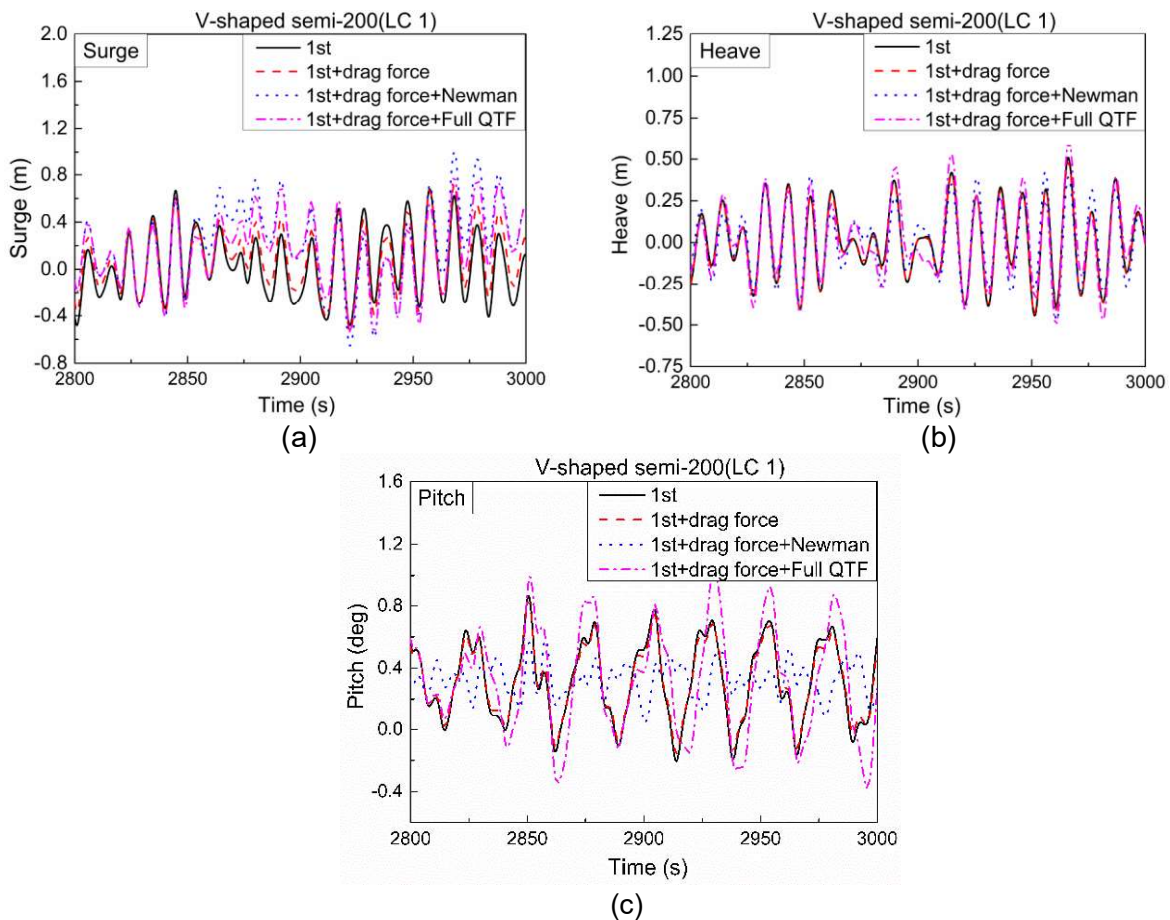


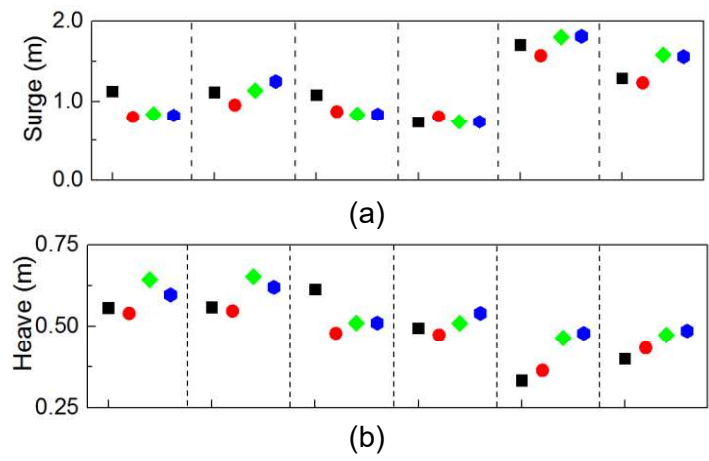
Figure 7. Time-domain motion response of the V-shaped semisubmersible FOWT in LC 1 condition. (a) Surge; (b) Heave; (c) Pitch.

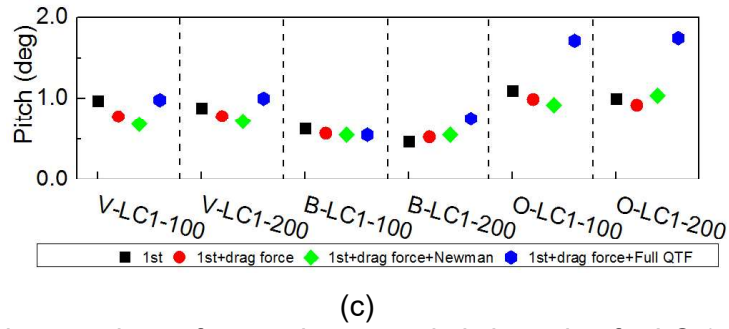
4.1 Time-domain analysis

4.1.1 Motion response

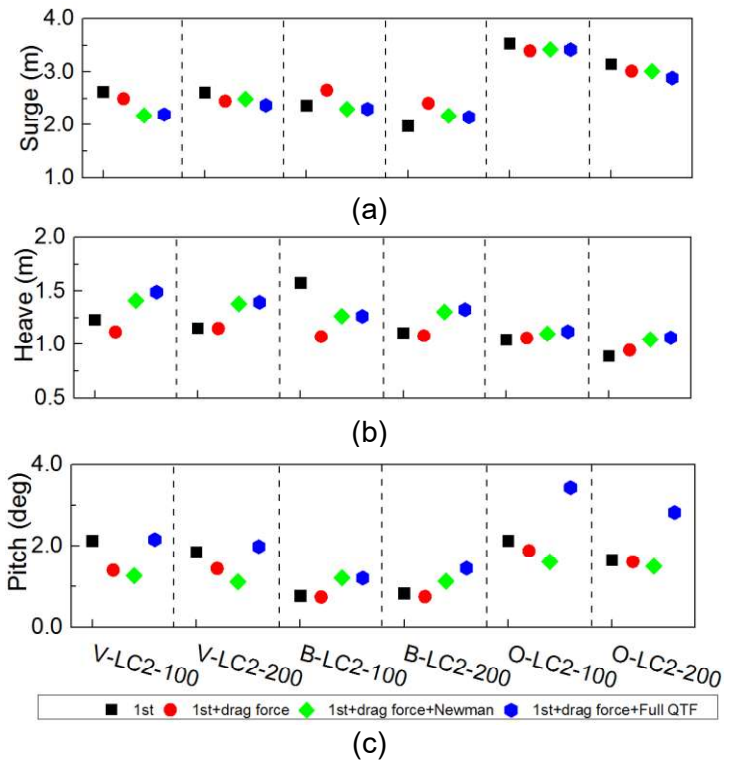
In this section, the time-domain dynamic motion responses of three platforms in different sea conditions with two water depths are estimated. In order to focus on the most critical motion response, only surge, heave and pitch motion are displayed. The total simulation time of the three semisubmersible FOWT is 3500 s, and the first 500 s have not been considered for either for drawing spectrum or statistical results to ignore the transient effect. Due to the limited space in this paper, only the motion time-domain response of the V-shaped semisubmersible FOWT under the LC 1 condition at a 200-m water depth is shown in Figure 7. Moreover, the statistical results of the three semisubmersible FOWTs are discussed in this section.

The effect of the Morison drag term and second-order difference frequency wave force, as well as water depth, were the main focal point. In Figures 8 to 10, the maximum oscillation amplitude of the second-order solution is plotted along with the first-order results.

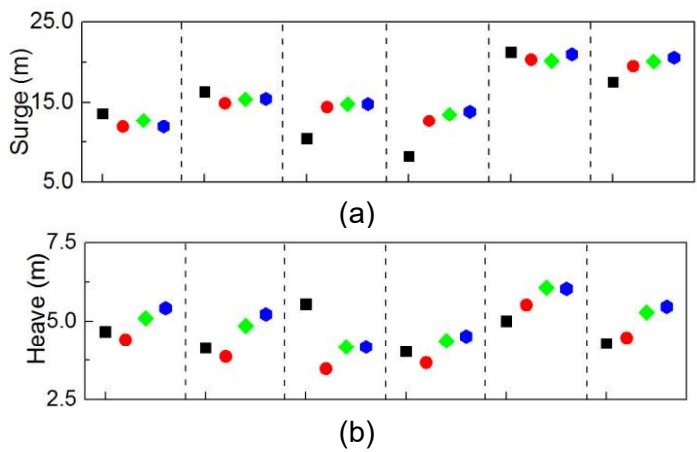




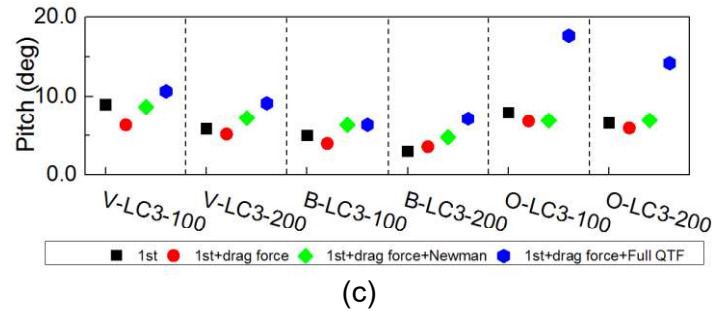
448
449
450 **Figure 8.** Maximum values of surge, heave and pitch motion for LC 1 condition. (a)
451 Surge; (b) Heave; (c) Pitch.



452
453
454
455
456
457
458 **Figure 9.** Maximum values of surge, heave and pitch motion for LC 2 condition. (a)
459 Surge; (b) Heave; (c) Pitch.



460
461
462
463



(c)
Figure 10. Maximum values of surge, heave and pitch motion for LC 3 condition. (a) Surge; (b) Heave; (c) Pitch.

The following conclusions can be drawn from Figures 8 to Figure 10:

For surge motion, the responses of the OC4-DeepCwind semisubmersible FOWT are larger than those of the other two platforms both at 100-m and 200-m water depths. The results of the first-order solutions show that maximum surge motion responses are larger than those considering the drag term effect for the V-shaped semisubmersible and OC4-DeepCwind semisubmersible FOWTs. For the second-order solution, the maximum surge motion responses are similar for the three semisubmersible FOWTs, showing that Newman's approximation solution considering the second-order effect is enough for the surge DOF.

For heave motion, the maximum motion response of the OC4-DeepCwind semisubmersible FOWT is lower than those of the other two platforms under moderate sea conditions, while it is larger than those of the other two platforms in extreme sea conditions. As shown in Figure 4(b), the RAOs of heave motion for the OC4-DeepCwind semisubmersible FOWT is lower than those for the other two FOWTs when the frequency is greater than 0.5 rad/s. Therefore, under moderate sea conditions where the wave frequency is greater than 0.5 rad/s, the responses of heave motion are lower for the OC4-DeepCwind semisubmersible FOWT than for the other two platforms. However, the wave peak period in the extreme sea state (LC 3) is close to the heave natural period of the OC4-DeepCwind semisubmersible FOWT, which excites the heave motion response of the OC4-DeepCwind semisubmersible FOWT. For the first-order solution, the Morison drag term has limited impact on the heave motion. For the second-order solution, the second-order wave force can greatly excite the heave motion response, while the difference in maximum heave motion responses between the solution from Newman's approximation solution and the full-QTF solution is small.

For the pitch motion, these figures also reveal that the second-order wave force effects are important responses concerning the first-order results. As seen in Figure 8(c), Figure 9(c) and Figure 10(c), the pitch responses of second-order solutions are larger than those of first-

order solutions, showing that the second-order wave forces should be thoroughly considered especially under extreme sea condition(LC 3). Compared with Newman's approximation method, the full-QTF method is more accurate for the calculation of second-order wave forces. As observed in the plots, the pitch motion responses can be greatly excited when using the full-QTF method, especially for the OC4-DeepCwind semisubmersible FOWT. Under extreme sea condition (LC 3), the amplitude of pitch motion is around 10 degrees, while those are almost 18 degrees for the OC4-DeepCwind semisubmersible FOWT. It also can be observed that the contribution of second-order wave forces to the pitch motion increasing when the water depth decreases. Therefore, full-QTF method is needed for the calculation of second-order wave forces to better capture the actual motion dynamic response for semisubmersible FOWTs.

For the moderate sea conditions, there is a great similarity regarding the standard deviation (STD); therefore, only the STD values from the LC 1 condition and LC 3 condition are listed. Tables 7 and 8 show the standard deviation (STD) results of the three semisubmersible FOWTs under different water depths in the LC 1 and LC 3 condition.

Table 7. STD values of motion response for the three semisubmersible FOWTs under LC 1.

Motion	Method	V-100- LC1	V-200- LC1	B-100- LC1	B-200- LC1	O-100- LC1	O-200- LC1
Surge	1st	0.32	0.30	0.32	0.22	0.47	0.45
	1st+drag force	0.24	0.25	0.24	0.23	0.36	0.36
	1st+drag force+Newman	0.27	0.31	0.26	0.24	0.44	0.44
	1st+drag force+Full QTF	0.27	0.30	0.27	0.25	0.45	0.45
Heave	1st	0.19	0.18	0.21	0.17	0.13	0.13
	1st+drag force	0.19	0.18	0.21	0.17	0.13	0.13
	1st+drag force+Newman	0.20	0.18	0.15	0.15	0.13	0.13
	1st+drag force+Full QTF	0.20	0.19	0.23	0.19	0.13	0.13
Pitch	1st	0.22	0.19	0.19	0.15	0.39	0.35
	1st+drag force	0.21	0.17	0.16	0.14	0.34	0.32
	1st+drag force+Newman	0.22	0.11	0.15	0.15	0.29	0.30
	1st+drag force+Full QTF	0.30	0.26	0.21	0.19	0.56	0.61

Table 8. STD values of motion response for the three semisubmersible FOWTs under LC 3.

Motion	Method	V-100- LC3	V-200- LC3	B-100- LC3	B-200- LC3	O-100- LC3	O-200- LC3
Surge	1st	3.73	3.77	3.18	2.05	6.49	4.40
	1st+drag force	2.90	3.15	2.95	2.54	4.16	3.79
	1st+drag force+Newman	2.76	3.34	3.36	2.92	4.06	4.08
	1st+drag force+Full QTF	2.71	3.24	3.49	3.00	4.08	4.00
Heave	1st	1.56	1.37	1.97	1.44	2.09	1.70
	1st+drag force	1.48	1.38	2.28	1.46	2.06	1.73
	1st+drag force+Newman	1.54	1.41	1.34	1.31	2.19	1.83
	1st+drag force+Full QTF	1.84	1.64	2.07	1.61	2.23	1.86

	1st	2.73	2.03	1.37	0.88	2.60	2.13
	1st+drag force	2.69	2.19	1.72	1.03	1.96	1.74
Pitch	1st+drag force+Newman	2.56	2.06	2.25	1.54	1.88	1.63
	1st+drag force+Full QTF	4.12	3.46	2.70	2.04	5.69	4.62

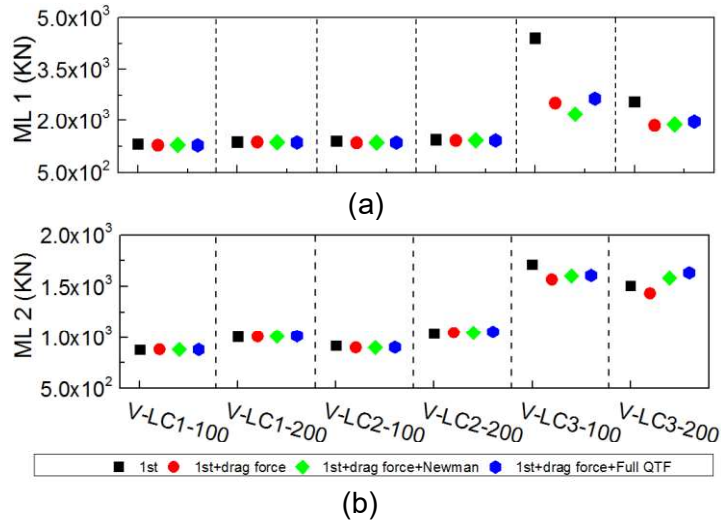
510 The surge motion response shows that the STD value of each semisubmersible FOWT is
511 larger when ignoring the Morison drag term. Comparing the results from different second-
512 order solutions, the maximum surge motion is similar for the three semisubmersible FOWTs.
513 These results indicate that together with the maximum values in surge motion, the accuracy
514 of the second-order wave force can be ensured in surge motion by using Newman's
515 approximation method. **Notably**, the Morison drag force applied to each column **is the**
516 **transverse drag force**. Therefore, it has little impact on the heave motion response as shown
517 in Tables 7 and 8. As it is can be observed in Tables 7 to Table 8, the STD value of the
518 heave motion response increased dramatically for the V-shaped semisubmersible and
519 Braceless semisubmersible FOWTs when using the full QTF method.

520 For the pitch motion, the STD values of three semisubmersible platforms changes
521 dramatically, especially for the OC4-DeepCwind semisubmersible FOWTs. Tables 7 and 8
522 also show that the STD value of the motion response is larger at a moderate water depth
523 than those at a water depth of 200 m, showing that the motion response of semisubmersible
524 FOWTs should be thoroughly considered at moderate water depths. **It is worth noting that**
525 **the STD value of pitch motion responses for the three semisubmersible FOWT is much**
526 **larger in full-QTF solution. Under extreme condition (LC 3), the STD value of pitch motion for**
527 **these three semisubmersible FOWT at 200 m water depth is increased by 67.0%, 32.0%**
528 **and 183.4% respectively when using the full-QTF method.** As we can see under the extreme
529 sea condition of the full QTF solution, **when** water depth decreases, the STD of the pitch
530 responses for the V-shaped semisubmersible, Braceless semisubmersible and OC4-
531 DeepCwind semisubmersible FOWT is increased by 19.08%, 32.35% and 23.16%
532 respectively, showing that the Braceless semisubmersible FOWT is more sensitive to the
533 change of water depth.

534 In general, the platform motion responses are larger when considering the second-order
535 force using the full QTF method. In other words, the maximum and STD values of the motion
536 responses indicate the need to calculate the second-order wave force accurately along with
537 the first-order loads to obtain the realistic combined effect of low-frequency wave loading on
538 the overall system dynamics, which is underestimated without considering the second-order
539 terms.

1
2
3
4
5
6
7
8
9
10
11
12
13
14
15
16
17
18
19
20
21
22
23
24
25
26
27
28
29
30
31
32
33
34
35
36
37
38
39
40
41
42
43
44
45
46
47
48
49
50
51
52
53
54
55
56
57
58
59
60
61
62
63
64
65

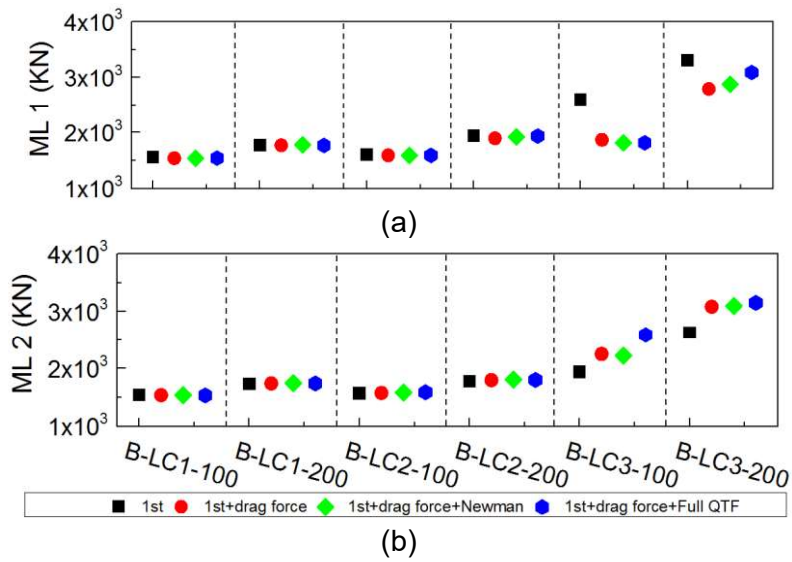
540
541



542
543
544

Figure 11. Maximum values of ML 1 and 2 for the V-shaped Semi. (a) ML 1; (b) ML 2.

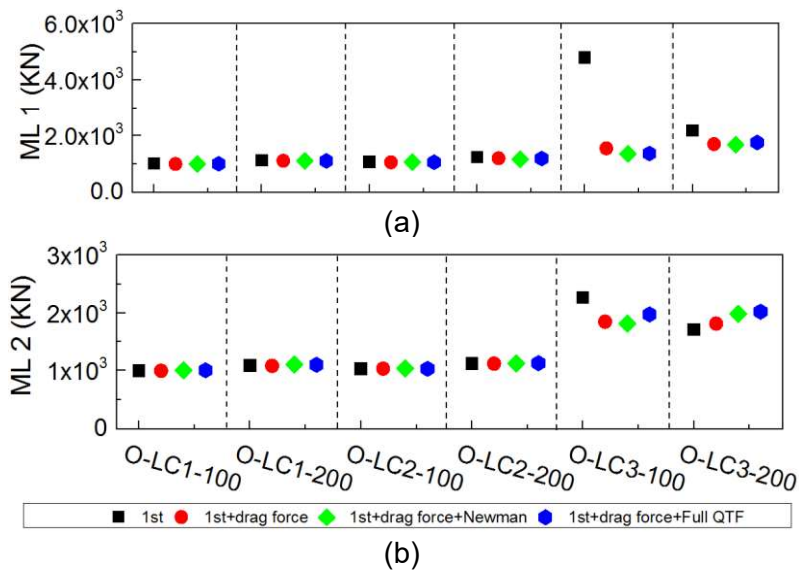
545
546



547
548
549

Figure 12. Maximum values of ML 1 and 2 for the Braceless Semi. (a) ML 1; (b) ML 2.

550
551



552
553
554

Figure 13. Maximum values of ML 1 and 2 for the OC4-DeepCwind Semi. (a) ML 1; (b) ML 2.

555 **4.1.2 Mooring tension response**

556 The maximum mooring line tensions for ML 1 and ML 2 are shown in Figure 11 to Figure 13.
 557 The standard deviation (STD) values of the mooring tension for the three semisubmersible
 558 FOWTs under the LC 1 and LC 3 conditions are shown in Table 9 and Table 10. Notably,
 559 there is a constant offset in the negative surge direction before reaching the static
 560 equilibrium for the V-shaped semisubmersible FOWT, while the Braceless and OC4-
 561 DeepCwind semisubmersible FOWTs do not have such an offset. Therefore, the pretension
 562 of ML 1 is larger than those of the other two mooring lines for the V-shaped semisubmersible
 563 FOWT.

564 The maximum values of the mooring line tension in extreme sea conditions, where the
 565 significant wave height is large, are relatively larger than those in moderate sea conditions
 566 for all semisubmersible FOWTs. The mooring line tension performance of the OC4-
 567 DeepCwind and V-shaped semisubmersible FOWT is similar at the two water depths, while
 568 the mooring line tension is larger at a water depth of 200 m than at a water depth of 100 m
 569 for the Braceless semisubmersible FOWT, as shown in Figure 11 to 13. Despite the small
 570 orders of magnitude for the drag force, it could reduce the motion response and then affect
 571 the mooring tension responses. As seen in the first-order solution, the maximum values and
 572 STD values of the mooring line tension are larger when ignoring the Morison drag force
 573 effect on the platform. Therefore, the drag term of the column should be thoroughly
 574 considered to better capture the actual mooring response for the three semisubmersible
 575 FOWT.

576 **Table 9.** STD values of the mooring tension responses for the three semisubmersible
 577 FOWTs under LC 1.

Tension	Method	V-100- LC1	V-200- LC1	B-100- LC1	B-200- LC1	O-100- LC1	O-200- LC1
ML 1	1st	32.20	22.94	18.04	24.96	16.74	24.58
	1st+drag force	28.48	22.27	13.01	25.41	11.73	21.58
	1st+drag force+Newman	29.02	22.54	13.92	25.53	15.04	23.24
	1st+drag force +Full QTF	29.32	22.55	14.74	26.33	15.42	23.89
ML 2	1st	20.62	17.66	12.38	18.68	8.74	12.33
	1st+drag force	20.06	17.55	10.68	18.81	6.41	10.88
	1st+drag force+Newman	20.46	17.96	11.04	19.08	8.24	12.34
	1st+drag force +Full QTF	20.46	17.96	11.29	19.31	8.42	12.65

579 **Table 10.** STD values of the mooring tension responses for the three semisubmersible
 580 FOWTs under LC 3.

Tension	Method	V-100- LC3	V-200- LC3	B-100- LC3	B-200- LC3	O-100- LC3	O-200- LC3
ML 1	1st	332.78	185.75	201.71	329.27	338.24	239.72
	1st+drag force	207.95	156.07	141.55	287.68	124.49	175.16
	1st+drag force+Newman	186.64	150.84	144.28	287.45	98.54	153.34
	1st+drag force +Full QTF	202.04	163.30	150.87	296.16	103.52	169.42
ML 2	1st	133.28	104.36	94.44	166.82	180.90	123.13
	1st+drag force	116.92	103.21	104.71	189.44	119.67	123.76
	1st+drag force+Newman	122.60	113.69	128.69	204.77	132.13	149.69
	1st+drag force +Full QTF	124.80	118.79	142.00	221.32	139.03	157.04

581 The second-order wave force could lead to large responses at resonance. Moreover, the
582 second-order wave force did increase the maximum values and standard deviation values.
583 As shown in Figures 10 to 12 and Tables 9 to 10, the maximum value, as well as the STD
584 values of **mooring force in a water depth of 100 m, is larger when using the full QTF method.**
585 Therefore, the effect of second-order wave force on the mooring line tension should be
586 thoroughly considered when designing semisubmersible FOWT and mooring systems for
587 moderate water depths.

588 From Tables 7, 8, 9 and 10, the STD results show that there is a good correlation between
589 the mooring tension and surge motion. Comparing the STD values for forces of ML 1 to
590 those for ML 2, 3 force reveals that ML 1 tension changed more dramatically than ML 2 and
591 3 tension for all semisubmersible FOWTs, which means that ML 1 is more sensitive to
592 external loads. These results show that ML 1 is more susceptible to fatigue damage than
593 other mooring lines and then causes the failure of the supporting platforms. For the mooring
594 system design of semisubmersible FOWTs, especially for triangular platforms, the main
595 mooring line should be strengthened to maintain the safety of the supporting structures.

596 4.2 Spectral analysis

597 This section presents the frequency-domain analysis results of the three semisubmersible
598 FOWT with a 0-degree incoming wave direction under three load cases at two water depths.
599 Four load models are listed together for comparison. The motion and mooring tension
600 responses with and without drag force on the column are compared. For the second-order
601 solution, the difference frequency wave loads using two methods (Newman's approximation
602 and the full QTF method) are obtained to investigate the second-order wave force effect on
603 the motion and mooring tension responses of semisubmersible FOWTs.

604 4.2.1 Natural frequencies of the three FOWTs

The natural frequency of the surge, heave and pitch motion for the three FOWTs are calculated by performing numerical decay tests in AQWA. Time series of free-decay tests on surge, heave and pitch motions can be obtained from AQWA output results. Then the natural frequency of the three FOWTs can be calculated based on the Fast Fourier Transform (FFT) method (Cooley *et al.*, 1969), as shown in Table 11.

Table 11. Natural frequency for the three semisubmersible FOWTs

Modes	V-shaped Semi	Braceless Semi	OC4-DeepCwind Semi
Surge (100/200 m) rad/s	0.086/0.067	0.080/0.083	0.058/0.050
Heave (100/200 m) rad/s	0.241/0.238	0.249/0.241	0.376/0.364
Pitch (100/200 m) rad/s	0.327/0.326	0.201/0.201	0.251/0.251

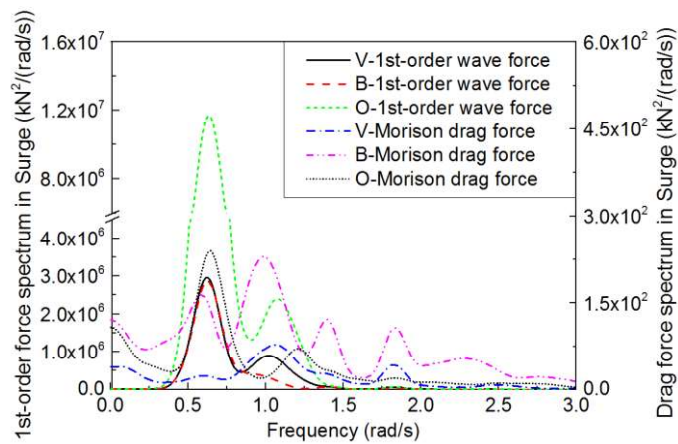


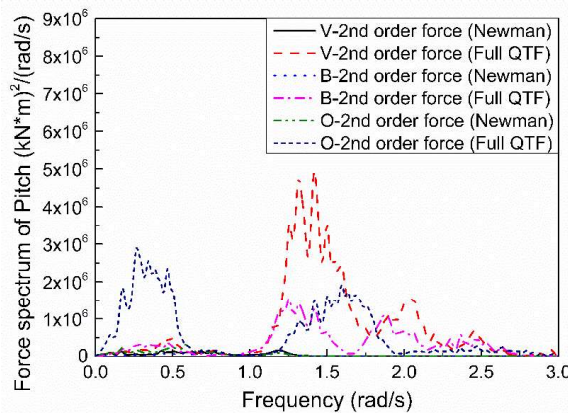
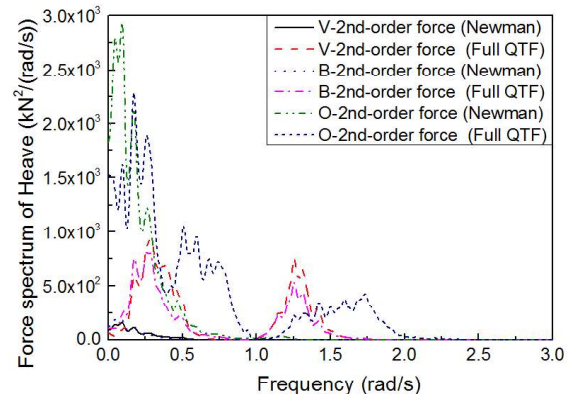
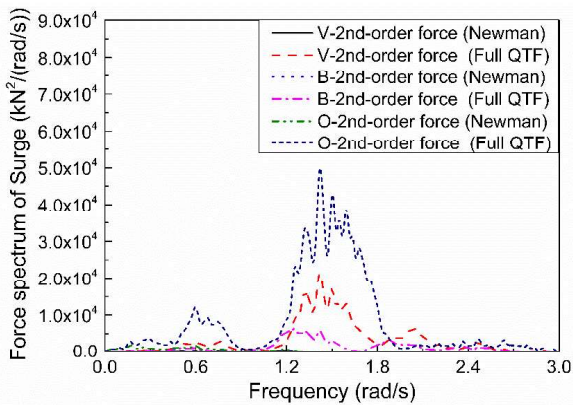
Figure 14. Comparison between drag force and first-order wave force (LC 1) in frequency domain of surge motion for the three semisubmersible FOWTs.

4.2.2 Hydrodynamic load spectrum

A comparison between the drag force and first-order wave force of the three semisubmersible FOWTs in the LC 1 condition at a 100-m water depth is shown in Figure 14. As shown in Figure 14, compared to the first-order wave force, the drag force is very small. Even though the drag force is small, its resonant effect can be significant. A comparison between the first-order wave force and drag force in the frequency-domain shows that the drag force is more broad-banded than the first-order force, which could cause large resonance in the low-frequency region especially for surge mode.

Figure 15 shows a comparison of the second-order wave force among the three semisubmersible FOWTs under moderate sea condition (LC 1) by using Newman's approximation and the full QTF method. The results show that the power spectral density is mainly concentrated in the difference-frequency region when using Newman's approximation,

626 while two peaks appear in the difference-frequency and sum-frequency region when using
 627 the full QTF method. Although the natural frequencies of the structure are designed to be
 628 outside the first-order wave energy spectrum, the second-order loads may excite these
 629 frequencies. **The difference-frequency is close to the natural frequency of the structures for**
 630 **semisubmersible FOWTs.** As shown in Figure 15(b), second-order responses in the
 631 difference-frequency region are higher when using the full QTF method than when using to
 632 Newman's approximation method of the V-shaped semisubmersible and Braceless
 633 semisubmersible FOWT, while the responses obtained using the two methods are similar for
 634 the OC4-DeepCwind semisubmersible FOWT. This set of data indicates that the second-
 635 order force calculated by the full QTF method can greatly excite heave motion response for
 636 the V-shaped semisubmersible and Braceless semisubmersible FOWTs. Figure 15(c) shows
 637 that, in the difference-frequency region, the second-order force responses computed using
 638 the full QTF method were higher than the responses computed using Newman's
 639 approximation method for the OC4-DeepCwind semisubmersible FOWT. The result
 640 indicates that the pitch motion of OC4-DeepCwind semisubmersible is more sensitive than
 641 that of the other two platforms when considering the second-order wave force.

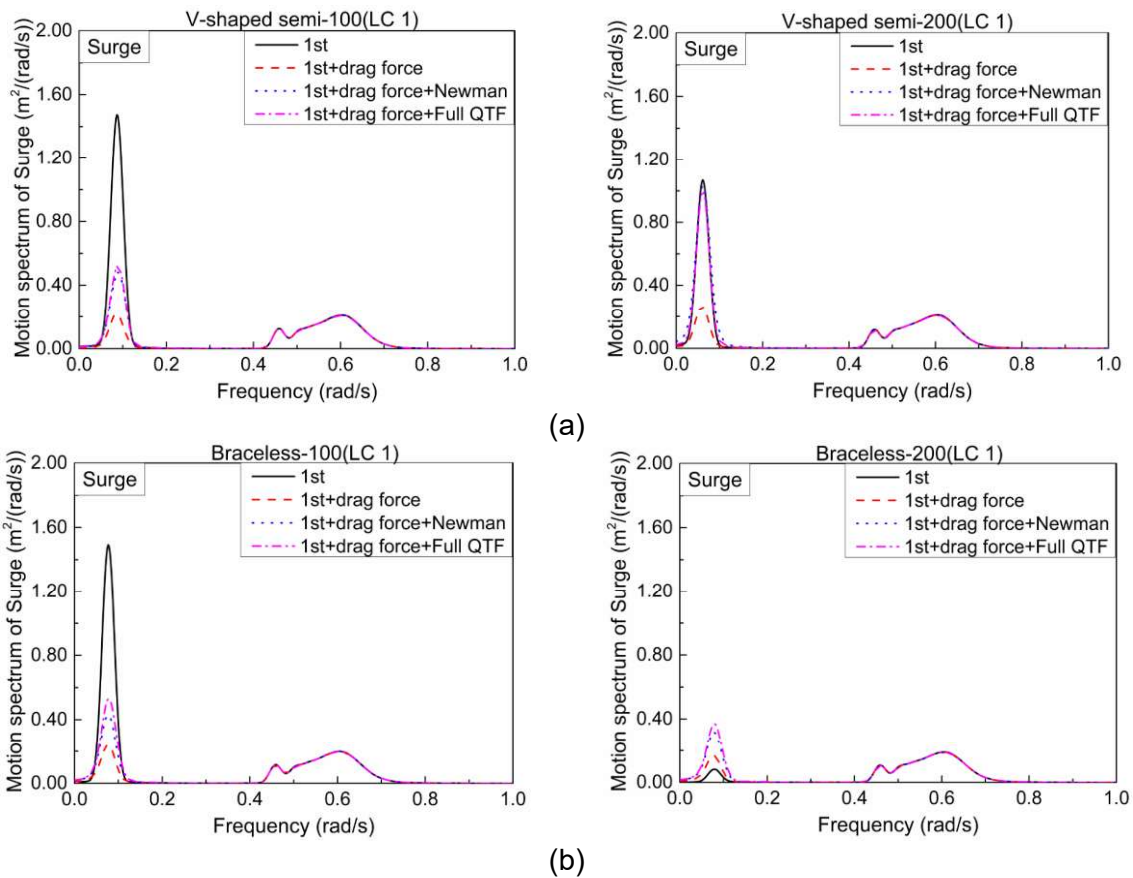


646 **Figure 15.** Comparison of the second-order wave force in the frequency-domain
 647 using different methods for the three semisubmersible FOWTs. (a) Surge; (b)
 648 Heave; (c) Pitch.

649 4.2.3 Motion spectrum

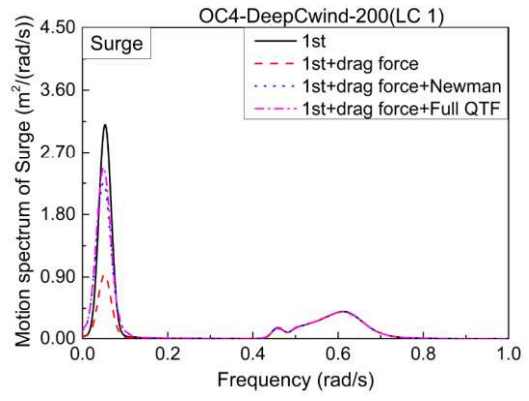
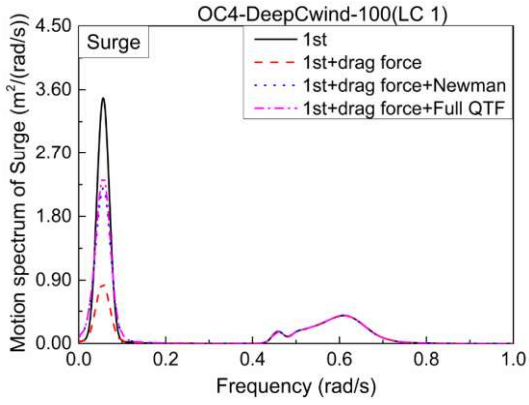
650 For moderate sea conditions, there is a great similarity regarding the power spectra density
 651 (PSD); therefore, only the spectrum results in the LC 1 condition are listed. Figure 16 to
 652 Figure 18 show the motion spectrum of the three semisubmersible FOWTs in the LC 1 at
 653 two water depths.

654 (1) For surge motion, the spectra of the motion responses consist of two parts: the low-
 655 frequency part is related to the surge natural frequency while the higher frequency part is
 656 dominated by the frequency from 0.4 to 0.8 rad/s which is related to the wave peak
 657 frequency. For the first-order solution, the surge resonance peak decreases significantly due
 658 to the drag force on each column compared to the first line as shown in Figure 16. This is
 659 similar to what is observed for the other platforms (Figure 16(b) and Figure 16(c)).



660
661

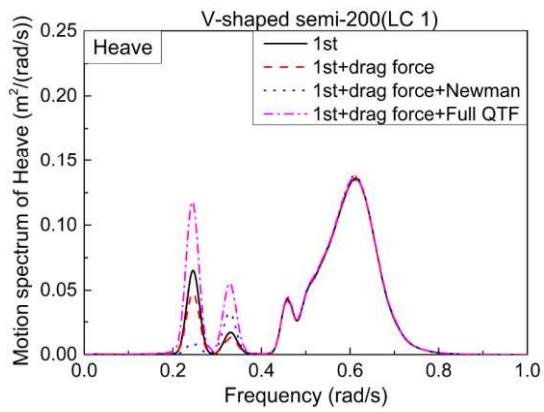
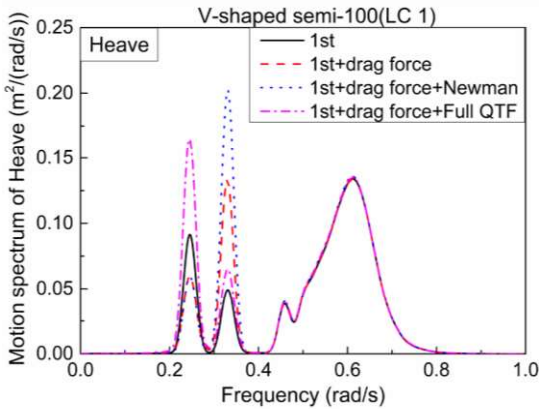
662
663



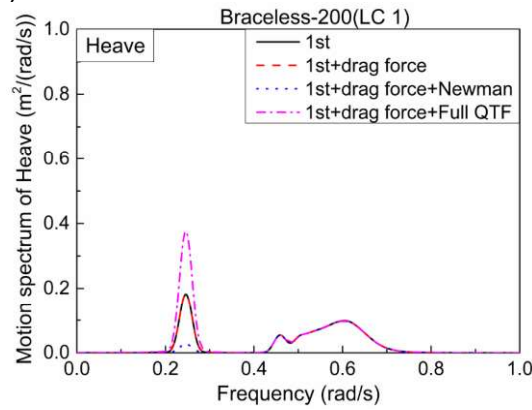
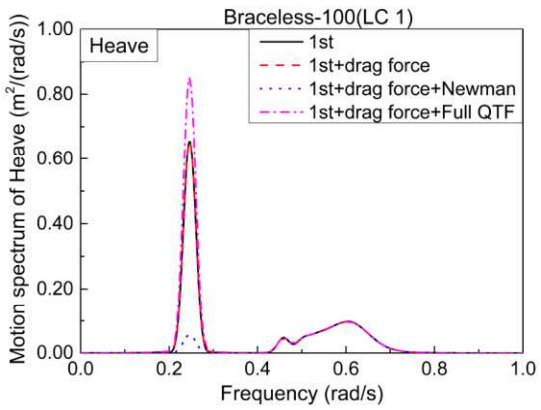
(c)

Figure 16. Floater surge motion spectrum of the semisubmersible FOWTs in LC 1 condition.

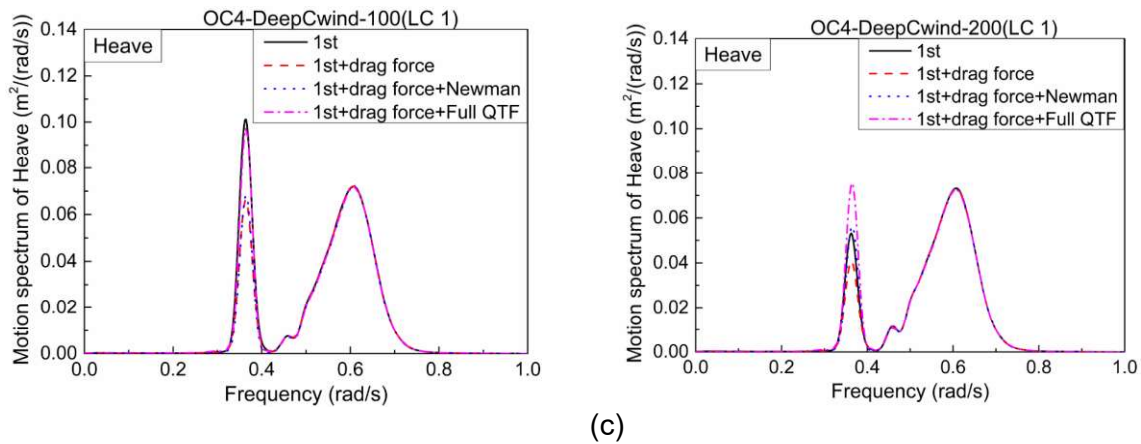
(a) V-shaped Semi; (b) Braceless Semi; (c) OC4-DeepCwind Semi.



(a)



(b)



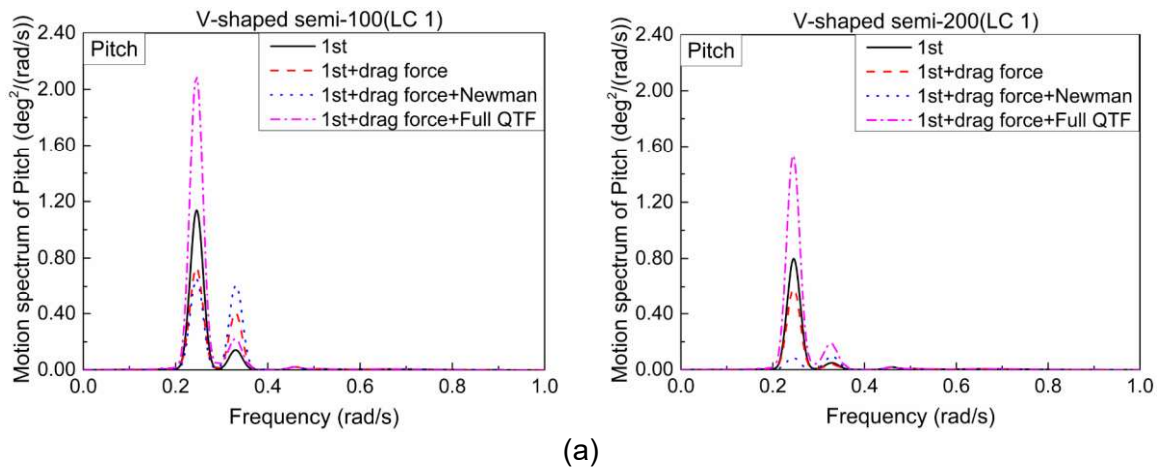
672
673
674 **Figure 17.** Floater heave motion spectrum of semisubmersible FOWTs in LC 1 condition. (a)
675 V-shaped Semi; (b) Braceless Semi; (c) OC4-DeepCwind Semi.

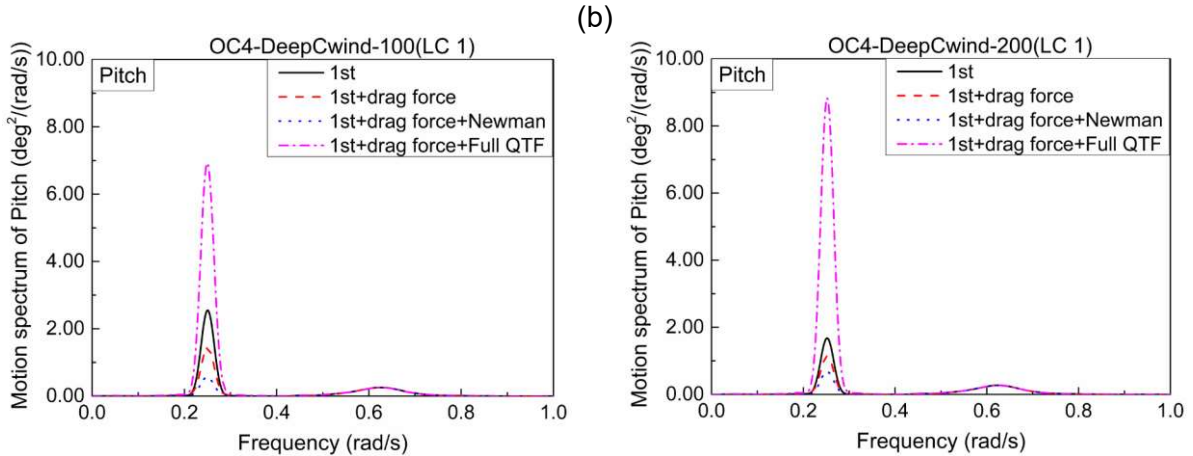
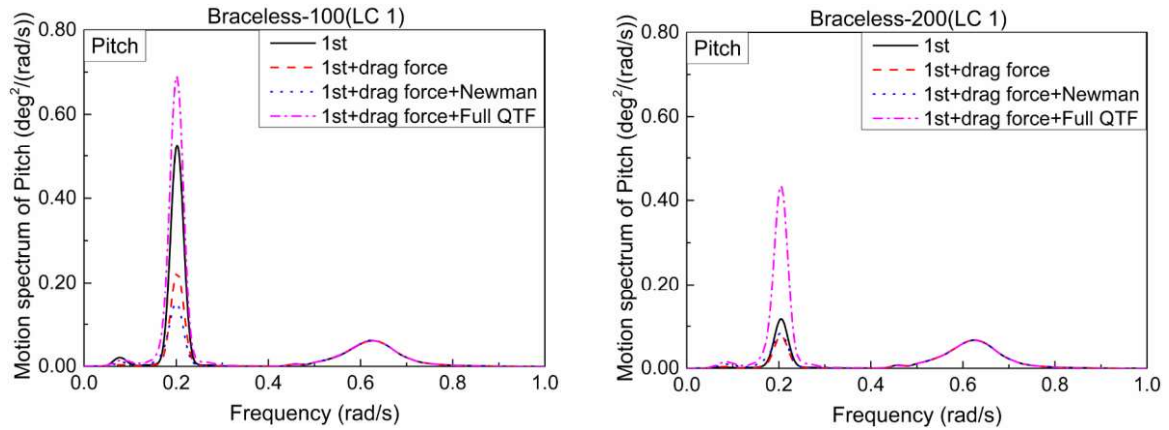
676 (2) For heave motion, the wave frequency response still dominates in the same range, which
677 is approximately 0.4 rad/s to 0.8 rad/s. A large response also occurs at the heave natural
678 frequency of each semisubmersible FOWT (Figure 17(b), Figure 17(c)). In contrast to the
679 other two semisubmersible platforms, the V-shaped semisubmersible FOWT exhibited two
680 peaks (Figure 17(a)), which are close to the pitch and heave natural frequencies, showing
681 the coupling between pitch and heave motions. It is also observed that the wave frequency
682 response is larger in the 100-m case than in the 200-m case. For the first-order solution, the
683 difference in the heave motion response among the three semisubmersible floating platforms
684 is small with and without the Morison drag force on the column. Comparing the difference-
685 frequency response obtained by using Newman's approximation and the full QTF method
686 clearly reveals that the heave motion response is underestimated for Newman's
687 approximation solution in the V-shaped semisubmersible FOWT and Braceless
688 semisubmersible FOWT (Figure 17(a) and Figure 17(b)). By contrast, for the OC4-
689 DeepCwind semisubmersible FOWT, the difference in the heave motion response between
690 Newman's approximation and the full QTF method is smaller than that for the other two
691 semisubmersible floating platforms.

692 (3) For pitch motion, different from the other modes, the spectra of the motion responses are
693 mainly dominated by the response at the pitch natural frequency. For the V-shaped
694 semisubmersible FOWT (Figure 18(a)), there are two peaks in the low-frequency region,
695 which are at the pitch and heave natural frequencies, showing the coupling effect of these
696 two modes. For the Braceless and OC4-DeepCwind semisubmersible FOWTs, the spectra
697 of the motion responses consist of two parts: the low-frequency part is related to the pitch
698 natural frequency while the higher frequency part is dominated by the frequency of 0.4 to 0.8
699 rad/s which is related to the wave peak frequency. For the second-order solution, the

700 difference-frequency wave force can greatly excite the resonance of the pitch mode
 701 response when using the full QTF method. As seen in the plots, the peak value at pitch
 702 natural frequency is higher in full-QTF solution, which causes large pitch responses for the
 703 three semisubmersible FOWTs as shown in Figures 8(c), 9(c) and 10(c).

704 Comparing the values with and without the drag force reveals that dynamic response of
 705 surge motion can be greatly decreased by adding the Morison drag force on the column.
 706 Therefore, it is vitally significant to consider the drag term when designing and performing
 707 the computation of semisubmersible FOWTs. Newman's approximation method is suitable
 708 for surge resonant motion response, while it doesn't apply to the heave or pitch resonant
 709 responses. It can be seen from Figures 16 and 17 that the heave and pitch resonant
 710 response in the low-frequency region is underestimated. Therefore, the full QTF method
 711 should be used for modelling the difference-frequency wave force to better simulate the low-
 712 frequency motion.

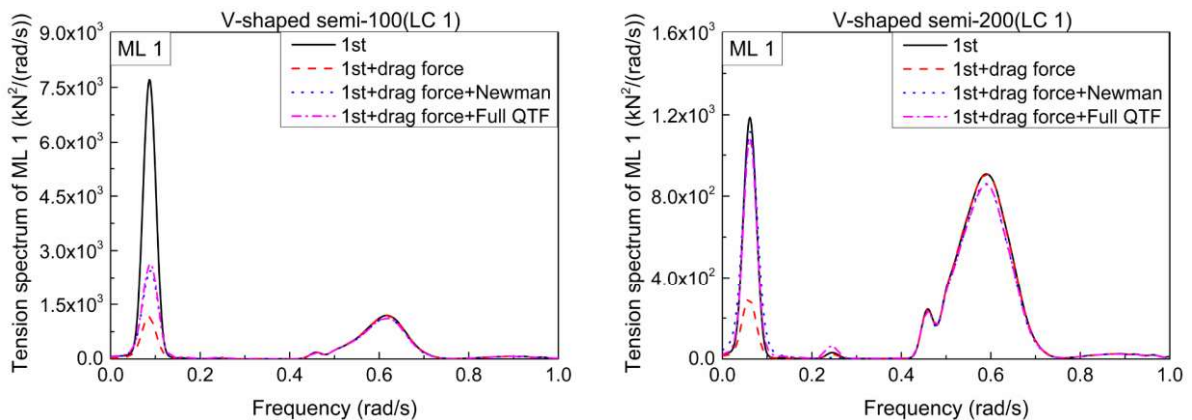




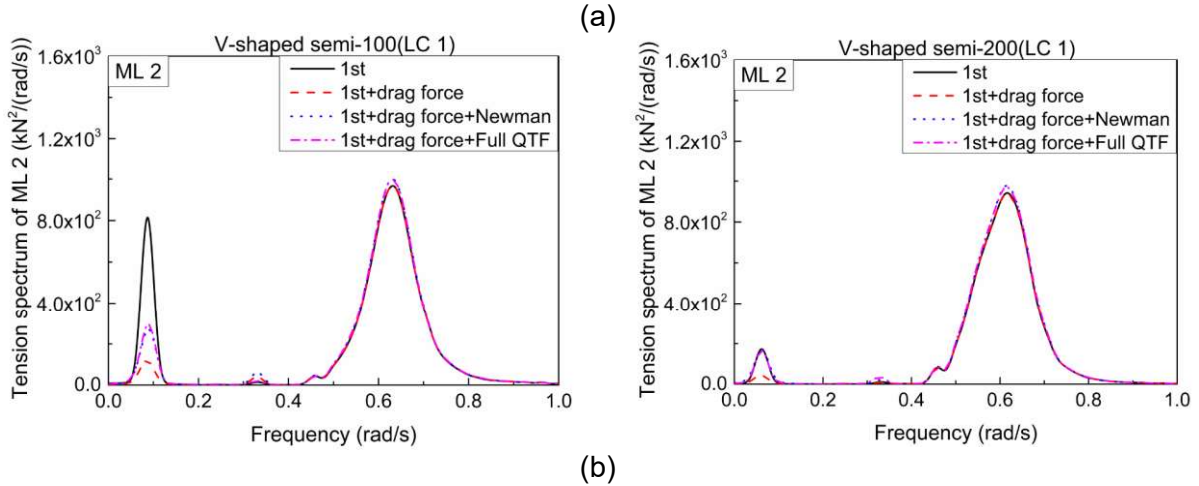
(c)
Figure 18. Floater motion spectrum of semisubmersible FOWTs in the LC 1 condition.
 (a) V-shaped Semi; (b) Braceless Semi; (c) OC4-DeepCwind Semi.

4.2.4 Mooring tension spectrum

The mooring line responses in the frequency domain in the head for sea under the LC 1 condition of the three semisubmersible FOWTs are shown in Figure 19 to 21. Due to the symmetry of the mooring line configuration of the three platforms, only the mooring line responses of ML 1 and ML 2 are displayed in this paper.



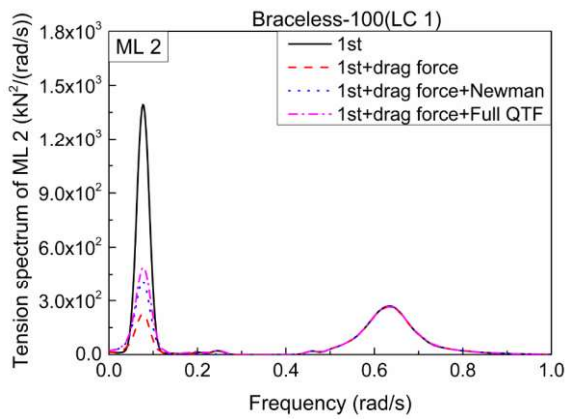
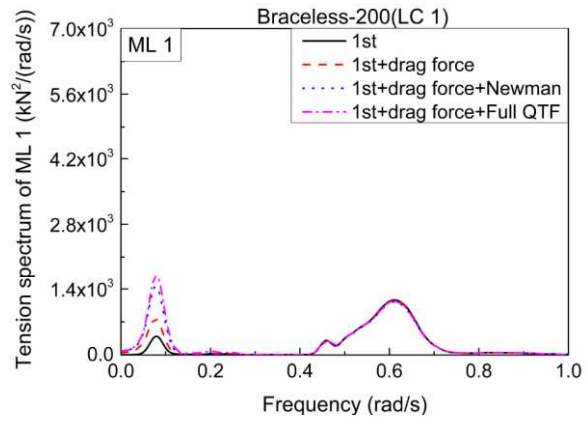
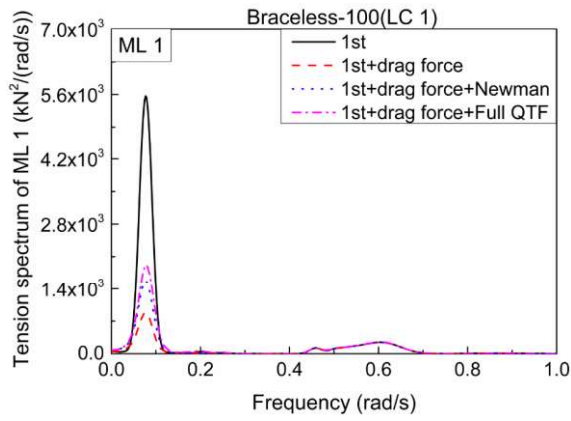
730



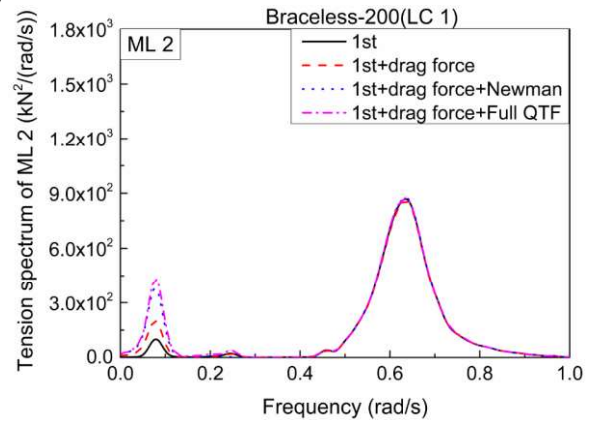
731
732
733 **Figure 19.** Mooring tension spectrum of the V-shaped Semi in LC 1 condition. (a) ML 1; (b)
734 ML 2.

735 For the V-shaped semisubmersible FOWT, the most significant contribution to the ML 1
736 tension comes from wave frequency range from 0.4 rad/s to 0.8 rad/s, while for ML 2 and 3,
737 the most significant contribution comes from the low-frequency region (surge motion
738 response). The contribution from the low-frequency response increases with decreasing
739 water depth. A small peak is observed at approximately 0.25 rad/s (pitch natural frequency)
740 showing the coupling effect between surge and pitch modes. The first-order solution results
741 show that the effect of drag force on the column becomes more significant as the water
742 depth decreased. It can also be seen that second-order surge resonant responses (Figure
743 19) seem similar when using the two methods to perform the calculations of the difference-
744 frequency wave force at both water depths.

745 For the Braceless semisubmersible FOWT, the mooring line tension responses consist of
746 two parts: the wave frequency range from 0.4 rad/s to 0.8 rad/s and the low-frequency region
747 including the surge, pitch and heave mode response. Similar to the V-shaped
748 semisubmersible FOWT, the contribution from the low-frequency response increases while
749 the high-frequency response (wave frequency) decreases. For the second-order solution,
750 the surge resonant responses are slightly higher when using the full QTF method than when
751 using the Newman's approximation to perform the difference-frequency wave force
752 calculation.



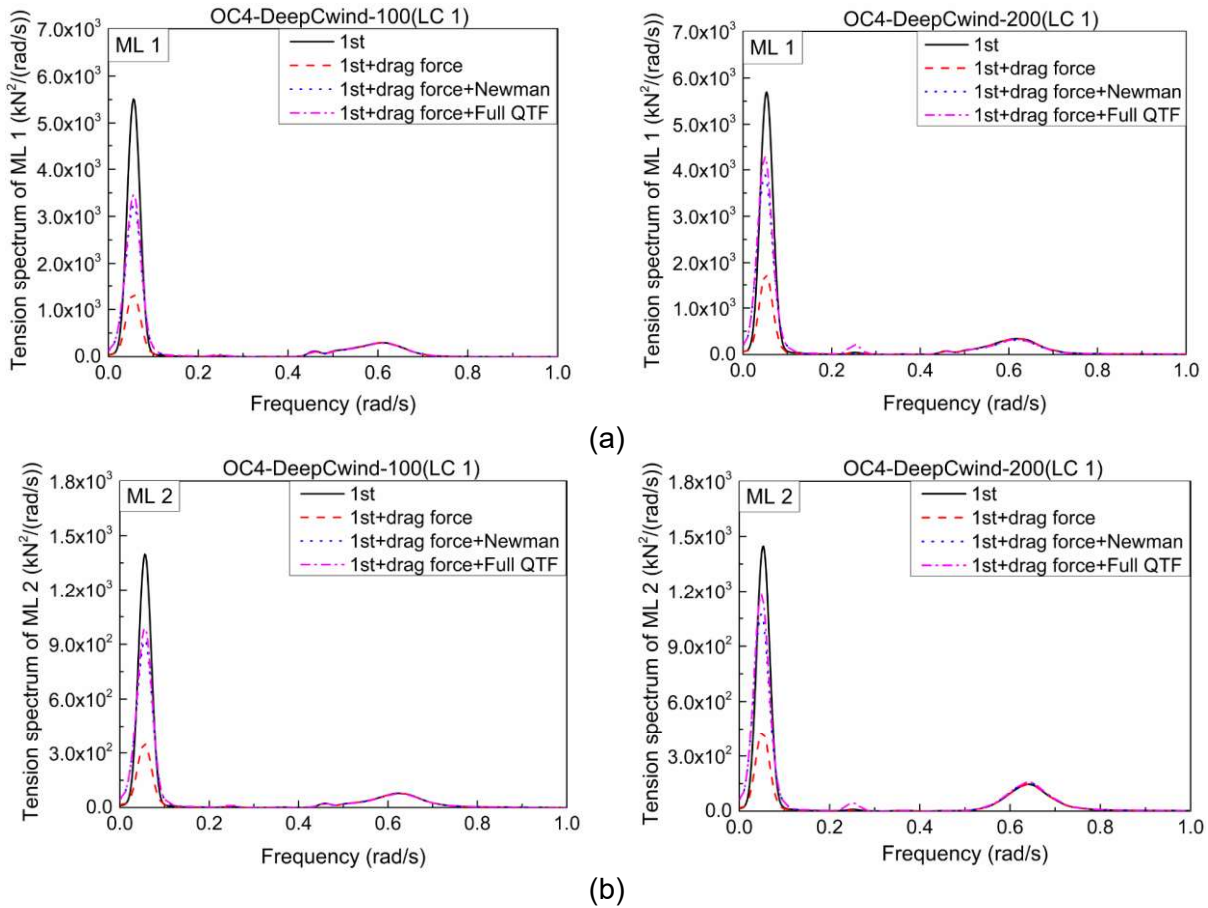
(a)



(b)

Figure 20. Mooring tension spectrum of the Braceless Semi in LC 1 condition. (a) ML 1; (b) ML 2.

For the OC4-DeepCwind semisubmersible FOWT, in contrast to the other two platforms, the most significant contribution to the mooring line tension comes from the low-frequency region. The coupling effect between structural modes, including the surge and pitch modes is shown in Figure 21. Compared to the other two platforms, the OC4-DeepCwind semisubmersible FOW show similar performance in the dynamic response of mooring line tension in the frequency-domain at the two water depth. Similar to the Braceless semisubmersible FOWT, surge resonant responses are slightly higher when using the full QTF method than when using Newman's approximation method to calculate the difference-frequency wave force.



769
770
771
772
773
774
775
776
777
778
779
780
781
782
783
784
785
786
787
788

Figure 21. Mooring tension spectrum of the OC4-DeepCwind Semi in the LC 1 condition. (a) ML 1; (b) ML 2.

5. Conclusions

In this paper, a comparative study of hydrodynamic performance among the V-shaped semisubmersible, Braceless semisubmersible and OC4-DeepCwind semisubmersible FOWT sunder different water depths is performed considering second-order hydrodynamic loads. Spectra and the time-domain response of platform motions and mooring tension are presented. The discussion has been made and useful conclusions can be summarized in the following aspects:

For the dynamic motion response, the result shows that the difference-frequency wave force can excite the responses at the natural frequency of all the semisubmersible FOWTs, especially for the pitch motion. Also, the results indicate that the pitch motion of OC4-DeepCwind semisubmersible FOWT is more sensitive than that of the other two semisubmersible FOWTs when considering the second-order wave loads. The STD value of the motion responses show that, compared with the Newman's approximation method, the STD values of pitch motion (LC 3) under water depth of 200 m for the semisubmersible

789 FOWTs, including the V-shaped semisubmersible FOWT, Braceless semisubmersible
790 FOWT and OC4-DeepCwind semisubmersible FOWT increased by 68.0%, 32.5% and 183.4%
791 respectively using the full-QTF method. Moreover, the first-order results show that the surge
792 motion response decreases when considering the Morison drag term on the column.
793 Therefore, the full QTF method is recommended to calculate the difference-frequency wave
794 force since the Newman's approximation could underestimate the motion response. Also,
795 the Morison drag term should be used for better simulating the actual motion responses.

796 The dynamic mooring tension response is mainly dominated by the response close to the
797 surge natural frequency and wave frequency range. Compared to mooring tension of ML 2
798 and ML 3, the STD values of the mooring tension show that ML 1 is more sensitive. For the
799 first-order solution, the mooring tension is overestimated when ignoring the Morison drag
800 term on the column. As it can be seen in Table 10, under the extreme sea condition, the
801 ML 1 tension of the V-shaped semisubmersible, Braceless semisubmersible and OC4-
802 DeepCwind semisubmersible FOWT is decreased by 16.0%, 12.9% and 26.9%, respectively,
803 in the water depth of 200 m. For the second-order solution, compared to Newman's
804 approximation solution, dynamic mooring tension response is more severe in the full QTF
805 solution.

806 For the dynamic response under different water depth, the results show that the motion and
807 mooring tension response is larger in the moderate water depth, which could cause fatigue
808 damage in long term and then threaten the safety of FOWTs. And the results also show that
809 the contribution of second-order wave forces increasing when the water depth decreases,
810 especially for pitch motion. The comparative results of the motion performance for three
811 semisubmersible FOWTs in different water depth showing that the Braceless
812 semisubmersible FOWT is more sensitive to the change of water depth. As shown in Figure
813 4, the heave motion response of OC4-DeepCwind semisubmersible is larger than that of the
814 other two semisubmersible FOWT for the extreme sea condition, for the reason that the
815 natural frequency of heave mode is close to the normal wave frequency range, which causes
816 large resonance in the OC4-DeepCwind semisubmersible FOWT. Therefore, the heave
817 natural frequency of the OC4-DeepCwind semisubmersible FOWT should be thoroughly
818 considered.

819 ACKNOWLEDGEMENT

820 This research was funded by the National Natural Science Foundation of China (Grant No.
821 51709039, 51709040). This work is also partially supported by the international collaboration

822 and exchange program from the NSFC-RCUK/EPSRC with grant No. 51761135011. This
823 work is also partially supported by LiaoNing Revitalization Talents Program (XLYC1807208)
824 and the Fundamental Research Funds for the Central University (DUT19GJ209).

825 **References**

826 DeCastro, M., Salvador, S., Gómez-Gesteira, M., Costoya, X., Carvalho, D., Sanz-Larruga,
827 F. J., and Gimeno, L. (2019). Europe, China and the United States: Three different
828 approaches to the development of offshore wind energy. *Renewable and Sustainable*
829 *Energy Reviews*, 109, 55-70.

830 Shi, W., Park, H. C., Chung, C. W., Shin, H. K., Kim, S. H., Lee, S. S., and Kim, C. W.
831 (2015). Soil-structure interaction on the response of jacket-type offshore wind
832 turbine. *International Journal of Precision Engineering and Manufacturing-Green*
833 *Technology*, 2(2), 139-148.

834 Shi, W., Tan, X., Gao, Z., and Moan, T. (2016). Numerical study of ice-induced loads and
835 responses of a monopile-type offshore wind turbine in parked and operating conditions. *Cold*
836 *Regions Sci Tech*, 123, 121-139.

837 Mo, R., Kang, H., Li, M., and Zhao, X. (2017). Seismic fragility analysis of monopile offshore
838 wind turbines under different operational conditions. *Energies*, 10(7), 1037.

839 Chian, C. Y., Zhao, Y. Q., Lin, T. Y., Nelson, B., and Huang, H. H. (2018). Comparative
840 study of time-domain fatigue assessments for an offshore wind turbine jacket substructure
841 by using conventional grid-based and Monte Carlo sampling methods. *Energies*, 11(11),
842 3112.

843 Hong, L., and Möller, B. (2011). Offshore wind energy potential in China: under technical,
844 spatial and economic constraints. *Energy*, 36(7), 4482-4491.

845 Driscoll, F., Jonkman, J., Robertson, A., Srinivas, S., Skaare, B., and Nielsen, F. G. (2016).
846 Validation of a FAST model of the statoil-hywind demo floating wind turbine. *Energy*
847 *Procedia*, 94, 3-19.

848 Maciel, J. G. (2010). *The WindFloat Project*. EDP: Lisbon, Portugal.

849 Bocard, N. (2014). The cost of nuclear electricity: France after Fukushima. *Energy*
850 *Policy*, 66, 450-461.

851 Skaare, B. (2017). Development of the hywind concept. In *ASME 2017 36th International*
852 *Conference on Ocean, Offshore and Arctic Engineering* . American Society of Mechanical
853 Engineers.

854 Roddier, D., Cermelli, C., Aubault, A., and Weinstein, A. (2010). WindFloat: A floating
855 foundation for offshore wind turbines. *Journal of renewable and sustainable energy*, 2(3),
856 033104.

857 Huijs, F., de Bruijn, R., and Savenije, F. (2014). Concept design verification of a semi-
858 submersible floating wind turbine using coupled simulations. *Energy Procedia*, 53, 2-12.

859 Lefranc, M., and Torud, A. (2011). Three wind turbines on one floating unit, feasibility, design
860 and cost. In *Offshore Technology Conference*. Offshore Technology Conference.

861 Le Boulluec, M., Ohana, J., Martin, A., and Houmard, A. (2013,). Tank testing of a new
862 concept of floating offshore wind turbine. In *ASME 2013 32nd international conference on*
863 *Ocean, offshore and arctic engineering*. American Society of Mechanical Engineers Digital
864 Collection.

865 Luan, C., Gao, Z., and Moan, T. (2016). Design and analysis of a braceless steel 5-mw
866 semi-submersible wind turbine. In *ASME 2016 35th International Conference on Ocean,*
867 *Offshore and Arctic Engineering*. American Society of Mechanical Engineers Digital
868 Collection.

869 Antonutti, R., Peyrard, C., Johanning, L., Incecik, A. and Ingram, D.(2016). The Effects of
870 Wind-Induced Inclination On the Dynamics of Semi-Submersible Floating Wind Turbines in
871 the Time Domain. *Renewable Energy*, 88, 83-94.

872 Jiang, Y., Hu, G., Jin, G., Sun, Z., Li, J. and Zong, Z.(2018). Hydrodynamic Performance of a
873 Novel Floating Foundation for Offshore Wind Turbine. *The 28th International Ocean and*
874 *Polar Engineering Conference*.

875 Shi, W., Zhang L., Ning, D., Jiang Z., Michailies, C., and Karimirad, M. (2019). A
876 comparative study on dynamic response of different semi floating offshore wind turbines.
877 In *ASME 2019 38th International Conference on Ocean, Offshore and Arctic Engineering*.
878 American Society of Mechanical Engineers.

879 Zhao, Z., Li, X., Wang, W., Shi, W., 2019. Analysis of Dynamic Characteristics of an Ultra-
880 Large Semi-Submersible Floating Wind Turbine. *Journal of Marine Science and Engineering*.

881 7(6), 169.

882 Roald, L., Jonkman, J., Robertson, A., Chokani, N., 2013. The Effect of Second-Order
883 Hydrodynamics On Floating Offshore Wind Turbines. *Energy Procedia*, 35, 253-264.

884 Coulling, A.J., Goupee, A.J., Robertson, A.N. and Jonkman, J.M.(2013). Importance of
885 Second-Order Difference-Frequency Wave-Diffraction Forces in the Validation of a Fast
886 Semi-Submersible Floating Wind Turbine Model. *ASME 2013 32nd International Conference
887 on Ocean, Offshore and Arctic Engineering*. American Society of Mechanical Engineers.

888 Li, J., Jiang, Y., Tang, Y., Qu, X., and Zhai, J. (2017). Effects of Second-Order Difference-
889 Frequency Wave Forces on Floating Wind Turbine under Survival Condition. *Transactions of
890 Tianjin University*, 23(2), 130-137.

891 Xu, K., Gao, Z., and Moan, T. (2018). Effect of hydrodynamic load modelling on the
892 response of floating wind turbines and its mooring system in small water depths. In *Journal
893 of Physics: Conference Series* (Vol. 1104, No. 1, p. 012006). IOP Publishing.

894 Gueydon, S., Duarte, T., and Jonkman, J. (2014). Comparison of second-order loads on a
895 semisubmersible floating wind turbine. In *ASME 2014 33rd International Conference on
896 Ocean, Offshore and Arctic Engineering*. American Society of Mechanical Engineers Digital
897 Collection.

898 Bayati, I., Jonkman, J., Robertson, A., and Platt, A. (2014). The effects of second-order
899 hydrodynamics on a semisubmersible floating offshore wind turbine. In *Journal of Physics:
900 Conference Series* (Vol. 524, No. 1, p. 012094). IOP Publishing.

901 ANSYS Inc. ANSYS AQWA, 2017, Line, Librium, NAUT and Tether Manuals; Pittsburgh, CO,
902 USA, 2017.

903 Faltinsen, O. (1993). *Sea loads on ships and offshore structures* (Vol. 1). Cambridge
904 university press.

905 Teng, B. *Wave action on maritime structures*, 3rd ed; Ocean press, Beijing, China, 2015.

906 Newman, J. T. (1967). The drift force and moment on ships in waves. *Journal of ship
907 research*, 11(01), 51-60.

908 Fonseca, N., Pessoa, J., and Guedes Soares, C. (2008). Calculation of second order drift
909 forces on a FLNG accounting for difference frequency components. In *ASME 2008 27th*

- 1
2
3
4
5
6
7
8
9
10
11
12
13
14
15
16
17
18
19
20
21
22
23
24
25
26
27
28
29
30
31
32
33
34
35
36
37
38
39
40
41
42
43
44
45
46
47
48
49
50
51
52
53
54
55
56
57
58
59
60
61
62
63
64
65
- 910 *International Conference on Ocean, Offshore and Arctic Engineering*. American Society of
911 Mechanical Engineers Digital Collection.
- 912 Pessoa J, Fonseca N, Guedes Soares C. (2010). Experimental and Numerical Study of the
913 Depth Effect on the First-order and Slowly Varying Motions of a Floating Body in Bichromatic
914 Waves. In *ASME 2010 29th International Conference on Ocean, Offshore and Arctic*
915 *Engineering*. American Society of Mechanical Engineers Digital Collection.
- 916 Pinkster, J. A. (1975). Low-frequency phenomena associated with vessels moored at
917 sea. *Society of Petroleum Engineers Journal*, 15(06), 487-494.
- 918 Hall, M., and Goupee, A. (2015). Validation of a lumped-mass mooring line model with
919 DeepCwind semisubmersible model test data. *Ocean Engineering*, 104, 590-603.
- 920 Jonkman, J., Butterfield, S., Musial, W., and Scott, G. (2009). *Definition of a 5-MW reference*
921 *wind turbine for offshore system development*. National Renewable Energy Laboratory.
- 922 Forward, F. (2014). *Fukushima Floating Offshore Wind Farm Demonstration Project*. Japan:
923 *Fukushima Offshore Wind Consortium*.
- 924 Karimirad, M., and Michailides, C. (2015). V-shaped semisubmersible offshore wind turbine:
925 An alternative concept for offshore wind technology. *Renewable Energy*, 83, 126-143.
- 926 Karimirad, M., and Michailides, C. (2016). V-shaped semisubmersible offshore wind turbine
927 subjected to misaligned wave and wind. *Journal of Renewable and Sustainable*
928 *Energy*, 8(2), 023305.
- 929 Borisade, F. (2016). Qualification of Innovative Floating Substructures for 10 MW Wind
930 Turbines and Water Depths Greater than 50 m—D 7.4: State-of-the-Art FOWT Design
931 Practice and Guidelines. *European Union*.
- 932 Luan, C. (2018). Design and analysis for a steel Braceless semi-submersible hull for
933 supporting a 5-MW horizontal axis wind turbine, PhD theses, Norwegian University of
934 Science and Technology, Trondheim, Norway, 2018.
- 935 Robertson, A., Jonkman, J., Masciola, M., Song, H., Goupee, A., Coulling, A., and Luan, C.
936 (2014) Definition of the semisubmersible floating system for phase II of OC4. National
937 Renewable Energy Laboratory.
- 938 Jeon, S. H. , Cho, Y. U. , Seo, M. W. , Cho, J. R. , and Jeong, W. B. (2013). Dynamic

939 response of floating substructure of spar-type offshore wind turbine with catenary mooring
1 940 cables. *Ocean Engineering*, 72, 356-364.
2
3
4 941 Li, L., Gao, Z., and Moan, T. (2015). Joint distribution of environmental condition at five
5 european offshore sites for design of combined wind and wave energy devices. *Journal of*
6 942 *Offshore Mechanics and Arctic Engineering*, 137(3), 031901.
7
8 943
9
10 944 Wind, G. L. (2005). Guideline for the certification of offshore wind turbines. *Germanischer*
11 945 *Lloyd Industrial Services GmbH*.
12
13
14 946 Cooley, J. W., Lewis, P. A., and Welch, P. D. (1969). The fast Fourier transform and its
15 applications. *IEEE Transactions on Education*, 12(1), 27-34.
16 947
17
18
19
20
21
22
23
24
25
26
27
28
29
30
31
32
33
34
35
36
37
38
39
40
41
42
43
44
45
46
47
48
49
50
51
52
53
54
55
56
57
58
59
60
61
62
63
64
65